UNIVERSIDAD DE CHILE
FACULTAD DE MEDICINA
ESCUELA DE POSTGRADO

“Effect of SARAF-based peptides on the store-operated calcium entry and cell invasion in triple-negative breast cancer model”.

MARÍA PAZ SALDÍAS MAULÉN

TESIS PARA OPTAR AL GRADO DE DOCTOR EN CIENCIAS BIOMÉDICAS

Director de Tesis: Prof. Dr. Oscar Cerda Arancibia

2023

UNIVERSIDAD DE CHILE
FACULTAD DE MEDICINA
ESCUELA DE POSTGRADO

INFORME DE APROBACION TESIS DE DOCTORADO EN CIENCIAS BIOMÉDICAS

Se informa a la Comisión de Grados Académicos de la Facultad de Medicina, que la Tesis de Doctorado en Ciencias Biomédicas presentada por el candidato

MARÍA PAZ SALDÍAS MAULÉN

ha sido aprobada por la Comisión Informante de Tesis como requisito para optar al Grado de **Doctor en Ciencias Biomédicas** en Examen de Defensa de Tesis rendido el día …… de …… de 2023.

Prof. Dr. Oscar Cerda A.
Director de Tesis
Instituto de Ciencias Biomédicas
Dpto. Biología Celular y Molecular
Facultad de Medicina, Universidad de Chile

COMISION INFORMANTE DE TESIS

PROF. DR. ELIAS LEIVA

PROF. DR. VICENTE TORRES

PROF. DR. GENARO BARRIENTOS

PROF. DR. HÉCTOR CONTRERAS
Presidente Comisión de Examen

Dedicado a mis amados pilares:
Padres María Cecilia y O. Gabriel, mi mayor regalo María José,
mi hermanito Gabriel, mis segundos padres María Ester y Mario
y mis fieles compañeras Tamy y Kira.

AGRADECIMIENTOS

Realizar un doctorado es una travesía compleja y desafiante que conlleva vivir en un vaivén de emociones y experiencias. Este viaje no solo desafía la capacidad intelectual, sino que pone a prueba la resistencia emocional. Los momentos de frustración, dudas e incertidumbre son inevitables. La presión para cumplir con los estándares de excelencia, así como la gestión del tiempo, pueden convertirse en grandes obstáculos en este camino. Sin embargo, la compañía de todos ustedes han hecho que este desafío sea un evento de transformación personal muy significativo que me ha permitido reencontrarme con ustedes y conmigo misma. Por esto les quiero expresar mi más profundo afecto y agradecimiento,

A mi mentor Oscar Cerda,

Por las oportunidades y herramientas que me ha brindado, sin duda la resiliencia y comunicación serán el sello de este proceso. Gracias a su exigencia y altos estándares, que me han impulsado a esforzarme al máximo y querer superar mis propias limitaciones. Gracias por el compromiso que usted ha tenido con el éxito de sus estudiantes y por sus enseñanzas y reflexiones, que llevaré conmigo siempre porque sé que éstas serán invaluables en mi futuro.

A mis colegas Pablo Cruz, Diego Maureira e Ian Silva,

Gracias por enseñarme trabajar en equipo, por su apoyo en todo momento, cariño y preocupación. Poder colaborar y aprender con ustedes ha sido una de las experiencias más enriquecedoras del doctorado. Gracias por los momentos de distracción, por escucharme y aconsejarme, todo esto fue un bálsamo en los momentos más desafiantes.

A los integrantes de Cerda Lab,

Gracias Rodrigo Santos, Octavio Orellana y Raquel Pinto, por todo su apoyo y trabajo, fueron parte esencial en este proyecto. Y todos los demás, gracias por su buena disposición y ayuda en los ensayos.

A mi amada familia y amigos,

No podría haber llegado tan lejos sin su amor incondicional, inquebrantable apoyo y sin su ejemplo de constante trabajo y esfuerzo. Durante estos años, su paciencia y comprensión fueron mi mayor fortaleza. Aprecio profundamente todo lo que han hecho por mí, por entender mis ausencias y por celebrar mis triunfos. Me siento enormemente afortunada y agradecida por tenerlos en mi vida.

A mi compañero de vida Boris Lavanderos,

Tu apoyo ha sido una fuente constante de fortaleza, esperanza y determinación, que me ha permitido superar momentos de duda y presión. Tu compañía ha hecho que los obstáculos parezcan menos intimidantes y que las victorias sean más dulces. Gracias por ser una increíble persona y por inspirarme cada día.

Por último a todos ustedes, este logro no es mío, sino el resultado de lo que cada uno me han entregado y por eso, es que tienen mi gratitud, admiración y cariño infinito.

FUNDING

This thesis is funded by:

- FONDECYT # 1200917 (Dr. Oscar Cerda)
- Millennium Nucleus of Ion Channel-Associated Diseases (MiNICAD), Iniciativa Científica Milenio, Agencia Nacional de Investigación y Desarrollo (ANID) (Dr. Oscar Cerda)
- Beca Doctorado Nacional ANID Folio Beca #21191141 (María Paz Saldías)
- Gastos Operacionales Beca Doctorado Nacional ANID (María Paz Saldías)

INDEX

ABSTRACT

Breast cancer is the most common cause of death among women. While there have been significant improvements in diagnosis and treatment, the spread of cancer to other areas of the body remains the primary reason for mortality. The triple-negative subtype of breast cancer is particularly aggressive and does not respond well to conventional therapies. Recent studies have shown that the influx of calcium through the Store-Operated Calcium Entry (SOCE) process plays a critical role in regulating cellular processes involved in the spread of breast cancer. This has made SOCE an interesting target for new therapies.

The SOCE-Associated Regulatory Factor (SARAF) has been identified as the primary regulator of the calcium-selective channel Orai, which is activated by STIM proteins. SARAF participates in the activation of the Orai1-STIM1 channel and subsequently contributes to its inhibition and potentiating Ca^{2+}-dependent inactivation mechanisms. Therefore, the interaction between SARAF and STIM1 is the primary molecular inhibitory checkpoint for SOCE regulation. However, the TNBC subtype exhibits a decrease in SARAF expression, and the C-terminal region of SARAF is sufficient to reduce the SOCE response. Based on this, we hypothesize that **SARAF-based peptides can inactivate STIM1, decreasing the SOCE response and the migration and invasion of triple-negative breast cancer cells.**

This proposal aims **to generate SARAF-based peptides that modulate the SOCE response, cell migration, and invasion in *in vitro* and *in vivo* models of triple-negative breast cancer.** This proposal comprises three specific aims:

Aim 1. Determine the functional effects of the C-terminal SARAF-based peptides as modulators of the SOCE response. To determine the functional effect of the C-terminal region of SARAF on the SOCE response, recordings of calcium dynamics were performed. Moreover, STIM1 clustering recording and BiFC complementation assays were performed, evidencing the effect of the C-SARAF fragments on the formation of the STIM1 cluster and STIM1-Orai1 complex respectively. In addition, the effect on the NFAT translocation from the cytoplasm to the nucleus is one of the main downstream targets activated by calcium signaling

associated with the SOCE response. Taken together, the data obtained suggest that the C-SARAF and C-SARAF^{K326R} fragments reduce the SOCE response, affecting the formation of the STIM1-Orai1 complex.

Aim 2. Determine the effect of the C-terminal SARAF-based peptides during cell migration and invasion in an *in vitro* model of triple-negative breast cancer. Migration and invasion assays were performed to evaluate the effect of these peptides on cellular processes involved in metastasis. In addition, focal adhesion dynamics were performed. The results obtained advise that the C-SARAF and C-SARAF^{K326R} fragments reduce cell migration and invasion affecting the dynamics of actin cytoskeleton rearrangement and assembly/disassembly of focal adhesions.

Aim 3. Determine the effect of the C-terminal SARAF-based peptides in the murine *in vivo* model of triple-negative breast cancer. *In vivo* murine models of tumor growth and metastasis of TNBC were performed. The histological analyses suggest that the overexpression of the C-SARAF and C-SARAF^{K326R} fragments reduces the invasion of tumor cells. Moreover, increases tumor lymphocytic infiltration, which constitutes a biomarker of good prognosis in the clinical context of TNBC.

Therefore, this study will contribute to the understanding of novel molecular mechanisms involved in Orai1-STIM1 activity. Moreover, the data acquired in this project could be directly applied to the design of new complementary drugs for cancer treatments.

Keywords: Triple-negative breast cancer, Store-Operated Calcium Entry, Cell migration, Cell invasion, C-terminal SARAF fragment.

INTRODUCTION

Breast cancer is the most frequent disease and is the leading cause of death in women worldwide and in Chile[1,2]. It is characterized by being a heterogeneous disease at the clinical, histopathological, and molecular levels, and hence its prognosis and treatment depend on the characteristics of the tumor[3]. Specifically, Triple-negative breast cancer (TNBC) represents 10-20% of all breast cancer, which is characterized to be the most aggressive subtype since the tumor lacks the expression of estrogen receptor, progesterone receptor, and human epidermal growth factor receptor 2 (HER2) proteins, so it does not respond to hormonal and HER2-targeted therapies[4]. Moreover, it is highly metastatic causing 90% of deaths [3,5]. Therefore, understanding the cellular and molecular bases involved during the metastatic process becomes relevant for the development of new and specific therapies that treat TNBC.

TRIPLE-NEGATIVE BREAST CANCER

TNBC presents different histological characteristics such as poor tumor differentiation, presence of metaplastic elements, medullary features, and stromal lymphocytic response [6]. Other histologic features are central necrosis, pushing tumor borders, and fibrosis[7,8]. In addition, TNBC is a heterogeneous subtype that includes intrinsic features of neoplastic cells (genomic[9], transcriptomic, and proteomic) and the extrinsic characteristics corresponding to the tumor microenvironment[4].

The tumor microenvironment is composed of cellular components that can be classified as local (intratumoral), regional (breast), and metastatic compartments. The local compartment corresponds to the biological features of the tumor cells and the tumor-infiltrating inflammatory cells[10]. Particularly, the inflammatory infiltrate or tumor-infiltrating lymphocytes (TILs), has reached a notorious relevance in the clinical and histopathological study of TNBC since it can provide prognostic information [11–13] and can be predictive of response to immunotherapy, chemotherapy, and other targeted therapies[14,15]. In this context, the microenvironment will influence the genetic and epigenetic alterations of neoplastic cells, allowing them to become invasive and disseminate from the primary site to distant locations, a process known as metastasis[16].

Metastasis is a complex pathological multi-step process[17] in which cancer cells lose their union with the extracellular matrix and with each other cells, to acquire migratory capacities and invade neighboring tissues [18]. Since metastasis causes 90% of deaths, understanding cellular and molecular mechanisms associated with cell migration and invasion are key to controlling this process [19] and developing future therapies against TNBC.

CELL MIGRATION

Cell migration is one of the key steps of metastasis and is regulated by a variety of concerted and dynamic mechanisms such as cytoskeletal rearrangement, focal adhesions (FA) turnover, and intracellular Ca^{2+} oscillations [20–23].

The cytoskeletal rearrangement is regulated by Rho GTPases proteins, such as Rac1 and Cdc42 that promote the formation of lamellipodia and filopodia respectively. While RhoA induces the polymerization of actin filaments and actin-myosin contractility[24]. These protrusions are stabilized by adhesion that links the actin cytoskeleton to the underlying extracellular matrix through integrin proteins[25]. Another relevant structure for cell migration is focal adhesion (FA). FAs are dynamic structures where their formation, maturation, and disassembly are a continuous process driven by the balance of actin polymerization and actomyosin contraction[25]. Therefore, the coordinated assembly and disassembly of FA and cytoskeleton rearrangement are essential for cell migration. In this context, Ca^{2+} is one of the most important secondary messengers. An increase in the levels of cytoplasmic Ca^{2+} is capable of triggering a wide variety of responses including the regulation of the assembly and disassembly of focal adhesions and rearrangement of the cytoskeleton[26].

Cytoplasmic Ca^{2+} homeostasis is maintained from two sources, internal Ca^{2+} storage (primarily the endoplasmic reticulum), and external Ca^{2+} influx. Different studies highlight the importance of the influx of Ca^{2+} through Store-Operated Calcium Entry (SOCE) response on the regulation of FA turnover[27], actin cytoskeleton dynamics, and cell migration[28]. Moreover, different groups have underlined the relevance of the SOCE response in various cancers such as melanoma[29–31],

glioblastoma[32], clear cell renal carcinoma[33], hepatocellular carcinoma [34], prostate cancer [31,35], cervical cancer[36], including breast cancer [37–40].

ACTIVATION AND REGULATION OF STORE-OPERATED CALCIUM ENTRY

SOCE is a predominant Ca^{2+} entry pathway in non-excitable cells, activated in response to a reduction in the intraluminal Ca^{2+} reservoirs of the ER. The pathway of activation of SOCE starts with the stimulation of membrane receptors that activate the Phospholipase type C, promoting PIP_2 hydrolysis to generate IP_3, which allows the IP_3-mediated Ca^{2+} release from the ER through IP_3R [41]. The main feature of SOCE is the Ca^{2+} Release Activated Current (I_{CRAC}) mediated by the dynamic interaction between the ER Ca^{2+} - sensing *stromal interaction molecule* proteins (STIM1 and STIM2)[42,43] and the Ca^{2+} selective, inward-rectifying Orai channels (Orai1, Orai2, and Orai3), located in the plasma membrane (PM)[44–47].

Under resting conditions, STIM1 and Orai1 proteins diffuse independently in the ER and PM, respectively [47]. When ER Ca^{2+} decreases, Ca^{2+} ions dissociate from the EF-hand motif of STIM generating a conformational change that allows its oligomerization, clustering, and subsequent translocation to ER-PM junctions and final spatial extension of the protein[48–51]. These structural changes include the release of the domain SOAR[47,53,54] from the autoinhibitory site[52], allowing its interaction with both N- and C-terminal regions of Orai1, triggering I_{CRAC} activation [53–57] and consequently Ca^{2+} entry into the cell[47,48,58].

I_{CRAC} is non-voltage-activated inwardly rectifying current. In addition, unitary conductance is approximately 10 fS, which is three orders of magnitude smaller than voltage-gated Ca^{2+} channels[45]. Moreover, it presents intrinsic and extrinsic mechanisms that control the inhibition of Orai channel activity and that are Ca^{2+}-dependent. There are two types of Ca^{2+}-dependent inactivation: Fast Ca^{2+}-Dependent Inactivation (FCDI) and Slow Ca^{2+}-Dependent Inactivation (SCDI). FCDI occurs within 10 and 100 ms[59–61], is triggered by Ca^{2+} that permeates through the channel and binds to specific regions within 10 nm of the pore and depending on a conserved negatively charged region in STIM1[61–64], STIM1-to-Orai1 expression ratio [65,66] and the calmodulin-binding domain of Orai1[61]. SCDI starts over 10 s and requires a rise in global cytosolic Ca^{2+} [67,68]. Slow inactivation can be mediated by mitochondrial Ca^{2+} buffering, CaM-

binding site in STIM1[69], and SOCE-associated regulatory factor (SARAF) [70,71], although a recent study showed that SARAF also participates in the FCDI[72]

STIM1 is an ER transmembrane protein with an ER luminal region encompassing an EF-hand motif that senses the luminal Ca^{2+} levels (K_d: 200–600 μM) [42,43]. and an α-sterile motifs (SAM) domain which is responsible for the oligomerization of the protein.[42,73]. On the other hand, the cytosolic region contains different key domains that contribute to both activation and inhibition of the SOCE response. The domains that participate in the activation of the response are two coiled-coil regions (called [49,55,76]CC2 and CC3) forming the STIM1-Orai1 Activating Region (SOAR) domain [47,48,74]. SOAR is the minimal sequence required for the activation of Orai1 and that binds to Orai1 through a polybasic lysine-rich region. Additionally, it contributes to STIM1 oligomerization[76] and it has recently been described that it directly interacts with phosphatidylinositol in the PM via a conserved lysine-rich site in the SOAR and is co-regulated by the STIM1 CC1 and ID domains. Apart from this, presents a polybasic lysine-rich region that mediates the interaction of STIM1 with $PI(4,5)P_2$[73,75,76]. On the contrary, CC1 contains an acidic region that is required for the action of the inhibitory helix that inhibits the SOAR domain and promotes the resting state of STIM [48,52,77]. Moreover, there is a C-terminal Inhibitory Domain (CTID) that mediates fast Ca^{2+}-dependent inactivation of Orai allowing the interaction of SOAR with the STIM1 inhibitory protein SOCE-Associated Regulatory Factor (SARAF) [70,71]

SARAF: A MASTER REGULATOR OF THE SOCE RESPONSE

Different effectors have been suggested as Orai1-STIM1 regulators[78–83]. However, SARAF constitutes the main regulator of Orai1-STIM1 channels[71]. SARAF was first described by Palty *et al.* (2012) and is a single transmembrane protein residing in the ER[71]. Currently, SARAF-STIM1 interaction is well documented and different studies showed that this interaction occurs at resting conditions[70,76,84,85] while upon ER Ca^{2+} depletion induces a transient decrease in the SARAF-STIM1 interaction, which re-associate after 1-2 min[76,85]. At a molecular level, Palty *et al.* (2012) determined that the N-terminal region of SARAF regulates its activity, while its C-terminal region interacts directly with the CTID domain of STIM1, facilitating the return of this protein to the resting state[70,71,86]. This effect is associated with slow Ca^{2+}-dependent

inactivation (SCDI) preventing Ca^{2+} overload [70,71]. Moreover, Zomot *et al.* (2021) show that SARAF also participates in SOCE activation upon ER Ca^{2+} depletion, facilitating the release of the SOAR domain of STIM1 and its subsequent activation, translocation to ER-PM junction, and Orai channel anchoring[72]. SARAF has a dual role in the STIM/Orai activity, initially participating in its activation and later in its inactivation.

TRIPLE-NEGATIVE BREAST CANCER AND SOCE RESPONSE

Yang *et al.* (2009) reported that decreased STIM1-Orai1 activity in MDA-MB-231 cells (human TNBC cell line) reduces cell invasion, while the overexpression of STIM1 and Orai1 in non-tumoral MCF-10A cell line promotes it [87]. Moreover, increased Orai1-STIM1 activity enhances the formation of podosomes and invadopodia, contributing to the invasive phenotype of breast cancer cells [31,35,40]. These reports suggest a robust and novel role for Orai1-STIM1, where increased expression and activity contribute to cancer progression and metastasis. Recently, Lee *et al* (2021) established the relevance of a positive modulator of the SOCE response in breast cancer progression. In addition, the use of an inhibitor of this regulator contributes to the reduction of the formation of focal adhesions and contraction of neoplastic cells [88]. Therefore, since fewer targeted medicines treat TNBC, understanding molecular mechanisms that regulate Orai-STIM activity will provide relevant information for the future development of new therapeutic strategies.

Although the SARAF interaction with STIM1 constitutes the main inhibitory molecular checkpoint for SOCE regulation, the mechanism of regulation of SARAF activity is still unknown. It has been proposed that the N-terminus of SARAF is responsible for the regulation of its inhibitory activity [71] acting as a switch that allows SARAF dimerization [89] while the C-terminal region recognizes a domain on STIM1 and is enough to reduce the SOCE response [71]. Therefore, understanding the mechanism of regulation of SARAF over STIM1 and SOCE will improve the knowledge to identify novel targets for breast cancer therapy.

To evaluate whether SARAF protein is correlated with breast cancer metastatic potential, we first consulted the TGCA NIH database using a widely used GEPIA platform[90]. We found that SARAF has no statistically significant changes in transcript

expression in tumors from patients in relation to non-tumoral tissue (Figure 1A). However, tumors molecularly classified as TNBC have diminished expression of SARAF concerning Luminal A (Figure 1B). Since TNBC tumors have high metastatic potential about other tumors[3], these data suggest that decreased SARAF expression could be contributing to increased SOCE response and highly migratory and invasive tumor phenotype**.**

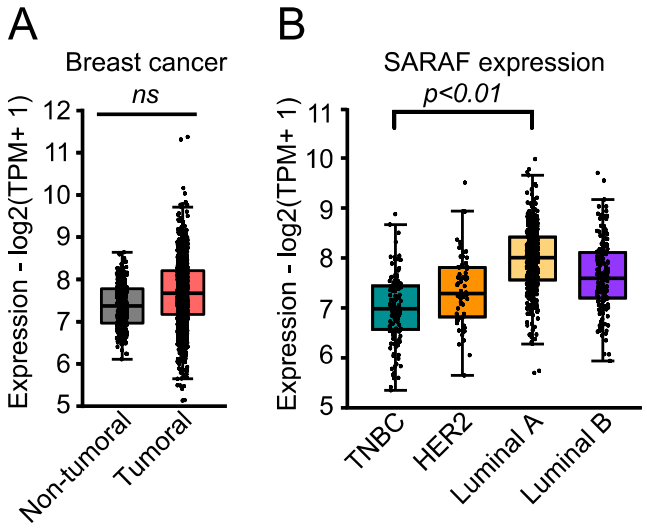

Figure 1. SARAF expression is decreased in triple-negative breast cancer.
A-B GEPIA analyses from the TGCA database. **A** Comparative graph of SARAF expression between tumoral and normal tissue. Number of samples in non-tumoral n=294, tumoral n=1084. **B** Comparative graph of SARAF expression between the different subtypes of breast cancer. The number of samples in TNBC samples n=135, HER2 n=66, luminal A n=415, and luminal B n=194. (Available at http://gepia2.cancer-pku.cn. Accessed on 26 June 2022).

Interestingly, in our laboratory, we have found a mutant version of SARAF in which lysine 326 has been replaced by an arginine residue which potentiates the negative regulator effect of the SOCE response (Figure 2). Therefore, the use of this version could have a protective effect on breast cancer.

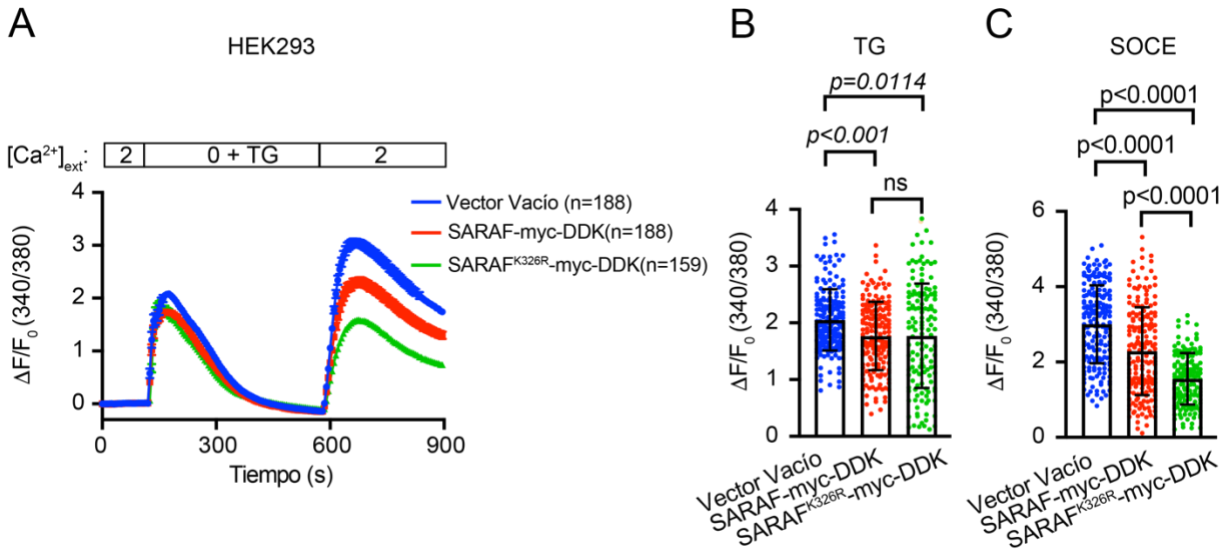

Figure 2. SARAF^{K326R} decreases the SOCE response in the HEK293 cell line.
A Representative graph of SOCE response. SARAF and SARAF^{K326R} were overexpressed in HEK293 cells which were loaded with Fura-2 AM and then Ca^{2+} imaging was performed. The protocol used consisted of 3 minutes with Ringer's solution of 2 mM $CaCl_2$, then Ca^{2+} depletion was induced with calcium-free Ringer's solution with 1 mM EGTA and 2 µM of thapsigargin (TG) for 7 minutes. Finally, the solution is changed to Ringer's 2 mM $CaCl_2$ to induce calcium entry. **B-C.** Representative graph of maximum peak TG-induced and maximum Ca^{2+} influx respectively. Figure obtained from Cruz, Maureira *et al.* (2024) (manuscript in preparation).

Based on the findings that the triple-negative subtype shows lower expression of the SARAF protein (as seen in Figure 1), which is the primary negative regulator of SOCE, and that this mechanism plays a crucial role in the progression of breast cancer, **Using the C-terminal region of SARAF to reduce calcium entry could be an effective treatment for TNBC by reducing STIM1-Orai1 activity, cell migration, and invasion of breast cancer cells.**

HYPOTHESIS

Since the C-terminal SARAF region interacts with STIM1 and is sufficient to regulate SOCE negatively, we hypothesize that: **"C-terminal SARAF-based peptides inactivate STIM1, decreasing the SOCE response and causing a reduction in cell migration and invasion of triple-negative breast cancer cells".**

GENERAL AIM

To generate C-terminal SARAF-based peptides that modulate the SOCE response, cell migration, and invasion *in vitro* and *in vivo* models of triple-negative breast cancer.

SPECIFIC AIMS

Aim 1. Determine the functional effects of the C-terminal SARAF-based peptides as modulators of the SOCE response.

Aim 2. Determine the effect of the C-terminal SARAF-based peptides during cell migration and invasion in *in vitro* model of triple-negative breast cancer.

Aim 3. Determine the effect of the C-terminal SARAF-based peptides in the murine *in vivo* model of triple-negative breast cancer.

MATERIALS AND METHODS

Cell culture and transfections

MDA-MB-231 (ATCC, HTB-26) cells were cultured in DMEM High Glucose media supplemented with 10% v/v FBS and 100 µg/mL penicillin-streptomycin. The 4T1 (ATCC, CRL-2539) cell line was cultured in RPMI media supplemented with 10% v/v FBS and 100 µg/mL penicillin-streptomycin. MDA-MB-231 cells were transfected using Lipofectamine LTX reagent (Thermo Fisher Scientific, Cat #15338100) and 4T1 cells were transfected with the different plasmids using Lipofectamine 2000 reagent (Thermo Fisher Scientific, Cat #11668019). All cell lines were grown at 37°C and 5% CO_2.

Stable lines of 4T1 cells that overexpress the fluorescent protein mScarlet and the fused proteins mScarlet-C-SARAF and mScarlet-C-SARAF^{K326R} were generated using the antibiotic G418 (Gibco, Cat #11811-031) at a concentration of 2 mg/mL. These cells were subsequently sorted at the REDECA facility (Faculty of Medicine, Universidad de Chile) using a FACSAria™ III Cell Sorter by selecting cells that exhibit red fluorescence for use in the in vivo metastasis experiments.

Plasmids

The plasmids used are summarized on Table 1.

Table 1. Plasmids.

Plasmid	Source	Catalog #	Amino acid sequence information
SARAF-Myc-DDK	Origene	RC201864	-
[2]SARAF^{K326R}-MYC-DDK	OC Lab	-	with substitution of lysine 326 by an arginine
mScarlet-H	Addgene	85043	-
[1]mScarlet-C-SARAF	OC Lab	-	cytosolic domain SARAF 135-339 aa

[1]mScarlet-C-SARAF^{K326R}	OC Lab	-	cytosolic domain SARAF with substitution of lysine 326 by an arginine
EGFPC1-huNFATc1EE-WT	Addgene	24219	-
pcDNA3-Venus-173-N-ORAI1	Addgene	87618	-
pcDNA3.1-STIM1-Venus-173-C	Addgene	87619	-
hSTIM1-YFP	Addgene	19754	
EGFP-Paxillin	Dr. Christopher Turner		

Cloning information: [1] Restriction enzyme, [2] Site-directed mutagenesis. All generated plasmids were sequenced.

mScarlet-C-SARAF cloning

SARAF-myc-DDK (Origene #RC201864) and SARAF^{K326R}-myc-DDK (obtained by site directed mutagenesis) were used as template for the amplification of the C-SARAF sequence. The C-terminal region of SARAF was considered the nucleotide sequence that corresponds from amino acid 195 to 339, according to the Uniprot database. Primers with restriction sites 5´-GAG CTC AAG ACG GGC AGT ATT CTC CTC CAC-3' and 5'-CTG CAG TTA TCG TCT CCT GGT AC-3' were designed to C-terminal SARAF sequence was incorporated in the plasmid pmScarlet-H_C1 (Addgene, Cat #85043).

Calcium Imaging

Cells were loaded with 5 µM Fura-2-AM for 30 min at room temperature. Then, cells were washed once and record with Ringer-Modified medium pH 7,40 containing 140 mM NaCl, 2.5 mM KCl, 10 mM Glucose, 2 mM $CaCl_2$, 1 mM $MgCl_2$, HEPES 10 mM. Free-Ca^{2+} Ringer-Modified medium containing 1 mM EGTA in absence of $CaCl_2$.

2 µM thapsigargin (TG) (Merck-Millipore, Cat #67526-95-8) was used for store Ca^{2+} depletion. Samples were excited using Halogen light source with alternated 340 nm and 380 nm excitation filters (Chroma). Fluorescence emissions at 510 nm were captured by Chameleon Camera (Chameleon CM3, Sony, Japan) every 5 s for frame using Eclipse Ti2-U inverted microscope (Nikon, Japan). SOCE protocol was performed in 4T1 and MDA-MB-231 and consists of 3 min of basal recording with modified Ringer's 2 mM $CaCl_2$, 7 min of reticular Ca^{2+} depletion using calcium-free Ringer's with TG to finally change the solution with modified Ringer's 2 mM $CaCl_2$ and recording for 5 min. Fluorescence intensity was quantified using the Image J/FIJI software (NIH, Bethesda, Maryland, US) and data were normalized by the initial ratio of fluorescence 340nm/380nm.

Biomolecular fluorescence complementation (BiFC)

BiFC assays were performed as described [91]. 4T1 cells were co-transfected with mScarlet, mScarlet-C-SARAF or mScarlet-C-SARAF^{K326R} and with pcDNA3.1-STIM1-Venus-173-C (Addgene, Cat #87619) and pcDNA3-Venus-173-N-ORAI1 (Addgene, Cat #87618) plasmids. Fourth-eight hours post-transfection, STIM1-Orai1 complementation was stimulated by the addition of 2 µM TG for 45 min at 37ºC in Ringer's solution modified 2 mM $CaCl_2$. Cells were fixed with fixative solution [4% w/v formaldehyde (freshly prepared from paraformaldehyde, Sigma-Aldrich, Cat #158127), 4% w/v sucrose (Sigma-Aldrich, Cat #S0389) in Dulbecco's phosphate buffered saline (DPBS), pH 7.4. After three washes for 10 minutes each, Hoechst 33342 nuclear stain at 200 ng/mL (Thermo Fisher Scientific, Cat #H3570) was performed. Samples were mounted with Fluoromount (Sigma-Aldrich, Cat #F4680). Images were acquired with 63X objective (N.A=1.35) using optical sectioning using structured illumination Zeiss Apotome 2, Axiovert 7. Particle density (particle number per cell area) and area were quantified using the Image J/FIJI software.

STIM1 clustering

STIM1 puncta formation was studied by Live-Cell Time-Lapse recordings using total internal reflection fluorescence microscopy (TIRF) providing high-resolution

images suitable for quantitative analysis [92,93]. This approach was performed in MDA-MB-231 cells cotransfected with hSTIM-YFP[94] and mScarlet, mScarlet-C-SARAF, or mScarlet-C-SARAF^{K326R}. The cells were seeded in fibronectin-coated coverslips (5 µg/mL). Images were acquired every 5 s for 125 frames using TIRFM 60X objective (N.A.=1.45) in an Olympus IX71 microscope (Tokyo, Japan) equipped with FLIR camera (Backfly S, BFS-U3-51S5M). Baseline recording was performed using modified Ringer's 2 mM $CaCl_2$ for 125 s. STIM1 puncta formation was induced by adding Free-Ca^{2+} Ringer-Modified medium containing 1 mM EGTA in absence of $CaCl_2$ and 2 µM thapsigargin (TG) (Merck-Millipore, Cat #67526-95-8) which was recorded for 500 seconds. Images were processed using ImageJ/FIJI software and FindFoci pluging[95] which allow the identification of peak intensity regions within 2D images. This process allows obtaining segmented images of recording with the individualization of STIM1 puncta. Then "analyze particles" was applied to obtain the number and area of the cluster in each image using circularity as a parameter with a value of 0.70-1.

NFAT translocation

MDA-MB-231 and 4T1 cells were cotransfected with mScarlet or mScarlet-C-SARAF and EGFPC1-huNFATc1EE-WT plasmids and then plated on polylysine-coated coverslips. Fourth-eight hours post-transfection cells were stimulated with 2 mM $CaCl_2$ modified Ringer's solution with 2 µM thapsigargine (TG) (Merck-Millipore, Cat #67526-95-8) for 45 minutes. Cells were fixed as described previously. Samples were mounted with Fluoromount (Sigma-Aldrich, Cat#F4680). Images were acquired with 63X objective (N.A=1.35) using optical sectioning using structured illumination Zeiss Apotome 2, Axiovert 7. Nuclear localization was confirmed by co-staining with the nuclear dye Hoechst 33342. [96]

Spreading assay

Spreading assays were performed as described [22]. MDA-MB-231 and 4T1 cells were transfected with mScarlet or mScarlet-C-SARAF or mScarlet-C-SARAF^{K326R}. Fourth-eight hours post-transfection were seeded on coverslips pre-coated with 5

μg/mL of Human plasma Fibronectin (Sigma-Aldrich, Cat #FC010). Briefly, cells were serum-starved for 16 h before assay. Then, 2 x 10^4 cells were seeded in 5 μg/mL fibronectin-coated 12 mm coverslips using a medium containing 10% v/v FBS. Ninety minutes post-seeding, cells were fixed as described previously. Then, cells were permeabilized and blocked with blocking solution (4% w/v non-fat dry milk/0.1% v/v Triton X-100 in DPBS) for 45 min at room temperature. Actin cytoskeleton was detected with Alexa-488-conjugated phalloidin (ThermoFisher, Cat #A12379). Nuclei were detected using Hoechst 33342 nuclear stain at 200 ng/mL (Thermo Fisher Scientific, Cat #H3570). Samples were mounted with Fluoromount (Sigma-Aldrich, Cat #F4680). Images were acquired with 63X objective (N.A.=1.35) using optical sectioning using structured illumination Zeiss Apotome 2, Axiovert 7.

Immunofluorescence: Focal adhesions

MDA-MB-231 cells were seeded on coverslips pre-coated with 5 μg/mL of Human plasma Fibronectin (Sigma-Aldrich, #FC010). Then, cells were incubated with HA-TAT-C-SARAF or HA-TAT-C-SARAF^{K326R} peptides. 24 hours post-incubation, cells were fixed as described previously. Then, cells were permeabilized and blocked with a blocking solution containing 0.1% v/v Triton X-100, and 4% w/v nonfat dry milk in DPBS, for 45 minutes at room temperature. Mouse anti-Vinculin IgG1 (Sigma-Aldrich, Cat #V4505) primary antibody in a 1:1000 dilution and rabbit anti-HA IgG1 in a 1:500 dilutions were incubated for 1 hour at room temperature. After three washes for 10 minutes each with blocking solution, Goat Alexa 488 – anti-mouse IgG1 secondary antibody and Goat Alexa 647- anti-rabbit IgG1 secondary antibody (ThermoFisher, Cat #A-21240) in a 1:1000 dilutions were used to mark focal adhesion spots and HA-TAT-peptides respectively. In addition, F-actin-stain phalloidin 555 in a dilution of 1:500 was used to mark the actin cytoskeleton. Hoechst 33342 nuclear stain at 200 ng/mL (Thermo Fisher Scientific, #H3570) was used. Samples were washed 3 times for 10 minutes each with DPBS solution and mounted with Fluoromount (Sigma Aldrich, Cat #F4680).

Images were acquired with 63X objective (N.A=1.35) using optical sectioning using structured illumination Zeiss Apotome 2, Axiovert 7. Images were processed using the Image J/FIJI software.

Focal adhesions dynamics

Focal adhesion (FA) turnover was studied by Live-Cell Time-Lapse recordings using total internal reflection fluorescence microscopy (TIRF) providing high-resolution images suitable for quantitative analysis [92,93]. This approach was performed in MDA-MB-231 cells cotransfected with EGFP-Paxillin and mScarlet, mScarlet-C-SARAF, or mScarlet-C-SARAF^{K326R}. The cells were seeded in fibronectin-coated coverslips (5 µg/mL). The cells were depleted from serum 48 h post-transfection for at least 3 h. FAs assembly/disassembly was induced by adding 10% v/v FBS in Modified Ringer's solution 2 mM $CaCl_2$. Images were acquired every 1 min for 30 frames using TIRFM 60X objective (N.A.=1.45) in an Olympus IX71 microscope (Tokyo, Japan) equipped with FLIR camera (Backfly S, BFS-U3-51S5M). Images were processed using ImageJ/FIJI software. FAs assembly and disassembly were visualized and quantified as the appearance or loss of fluorescence in a region of interest, according to Goetz *et al.* (2008) [97]. The assembly and disassembly rates were calculated by plotting the values of $\ln I/I_0$ versus time, according to what has been done in previous publications of the laboratory [93,98,99]

Transwell chamber invasion assay

MDA-MB-231 and 4T1 cells (5×10^4 cells) transfected with mScarlet, mScarlet-C-SARAF, or mScarlet-C-SARAF^{K326R} were plated into 8 µm pore-Transwell® chambers (Sigma-Aldrich, Cat #CLS3422). Transwell® chambers were preincubated with Matrigel (Sigma-Aldrich, Cat #E1270) overnight at 4°C and then they were placed for 30 min at 37°C before seeding the cells. Cell invasion was induced by adding 10% v/v FBS in the lower chamber for 16 hours at 37°C. The non-invasive cells were removed, and the invading cells were fixed and stained with 0.2% w/v crystal violet dissolved in 10% v/v methanol. The invading cells were counted and expressed as a percentage of control.

Scratch assay

MDA-MB-231 and 4T1 cells transfected with mScarlet, mScarlet-C-SARAF or mScarlet-C-SARAF^{K326R} were seeded on coverslips pre-coated with 5 μg/mL of Human plasma Fibronectin (Sigma-Aldrich, Cat #FC010) forming a monolayer. After 24 h, cells were depleted of serum for 4 h, and then wounds were made with a sterile micropipette tip (p200). Detached cells were removed by washing three times with DPBS, then the medium was replaced with DMEM 2% FBS (to promote cell migration) and three images were obtained from each wound (t_{0h}) with an inverted microscope. After 16 h, cells were fixed for 15 minutes at 4°C in fixative solution [4% w/v formaldehyde (freshly prepared from paraformaldehyde, Sigma-Aldrich, Cat#158127), 4% w/v sucrose (Sigma-Aldrich, Cat#S0389) in Dulbecco's phosphate buffered saline (DPBS), pH 7.4] and three images were obtained from each wound (t_{16h}). The relative sizes of the wounds at t_{0h} and t_{16h} were obtained using a wound healing size plugin of the ImageJ software and results were expressed as a percentage of closing ([(Area t_{0h} – Area t_{16h})/ Area t_{0h}]x100).

In vivo tumoral growth model

Stable cell line of 4T1 that express mScarlet, mScarlet-C-SARAF, or mScarlet-C-SARAF^{K326R} were injected associated with the animal protocol 20382-MED-UCH, approved by the Bioethics Committee of the Faculty of Medicine, University of Chile. Female Balb/c mice will be orthotopically injected into the fatty tissue of the fourth mammary gland (inguinal area) with stable cell line 4T1. Cells will be resuspended in phosphate buffered saline with 0.04% trypan blue (2 x 10^5 cells, 50 µL)[100].The general condition of the animals was evaluated daily according to the modified monitoring protocols of Morton and Griffiths (Veterinary Record, 116: 431-36, 1985). The mice were maintained for 21 days or when the score was equal to or greater than 15. Tumor growth was assessed postmortem. Once the tumor was extracted, three diameters (width, length, and height) of the ellipsoid were measured using a caliper, and the following formula was used to calculate the tumor volume [101]:

$$V_{ellipsoid} = \frac{4}{3}\pi \cdot \frac{w}{2} \cdot \frac{l}{2} \cdot \frac{h}{2}$$

w= width, l= length, h=height

Additionally, organs were removed, fixed, and processed for histological analysis and evaluation of metastatic sites.

Histology

The main organs that are affected during cancer metastasis either by indirect effect of primary tumor growth or by direct effect of the metastatic model (injection of tumor cells in the tail) were removed, washed with DPBS, and fixed with 4% w/v formaldehyde/ 4% w/v sucrose during 24 h at 4°C. Subsequently, the tissue was processed with increasing concentrations of alcohol, cleared with xylol, and embedded in paraffin.

Serial sections with a thickness of 3 μm was obtained and adhered to slides for histological Hematoxylin and eosin staining, Masson's trichrome and positively charged slides (Epic Scientific, +ASSURE+) for immunofluorescence.

Brightfield sample images were acquired with a Leica DFC425C camera installed on a Leica DM2500 CCD microscope with 10X and 40X objectives (Leica, Wetzlar, Germany).

Inflammatory infiltrate analysis.

TILs can be measured in slides stained with hematoxylin and eosin, presenting variation in density and location in the tumor[11,102]. Primary tumor samples were stained with Masson Trichromic and scanned using a Nanozoomer-XR digital slide scanner C12000 (Hamamatsu Photonics KK, Japan). TILs are reported as area occupied by mononuclear inflammatory cells over total intratumoral stromal area, where all mononuclear cells (including lymphocytes and plasma cells) should be scored, but polymorphonuclear leukocytes are excluded[102]. The images were analyzed by NDP.view software version 5.0.4.1382. This software allows us to quantify the TIL area expressed as mm^2.

Statistical Analyses

Data shown correspond to the mean ± SD or mean ± SEM of at least four independent experiments as indicated in the figure legends. Before the statistical analysis, the data groups were analyzed using a normality test, to evaluate the Gaussian distribution of the data. If the data present a normal distribution, analysis of variance (ANOVA) was applied following the same criterion of the normal distribution of the data. In addition, for data that do not have a Gaussian distribution, a non-parametric test was applied to correspond to Dunn's multiple comparisons test. To establish a significant difference between data sets, a value of $p<0.05$ was defined. The data was plotted following the structure of a SuperPlot[103]. This method allows observing the distribution of each independent experiment, with its respective average. Data were processed and graphed using Prism v.9.0 (Software GraphPad, CA, USA).

RESULTS

To find a peptide that reduces the SOCE response and the highly metastatic phenotype of TNBC, we propose the use of mScarlet-C-SARAF and mScarlet-C-SARAF^{K326R}) as potential modulators of SOCE. In our laboratory, we cloned the C-terminal fragment of SARAF, considering the nucleotide sequence that corresponds from amino acids 195 to 339[71]. This fragment was inserted into the plasmid with mScarlet by using restriction enzymes. These plasmids were overexpressed in the MDA-MB-231 and 4T1 cells to carry out the experiments described below.

AIM 1. DETERMINE THE FUNCTIONAL EFFECTS OF THE C-TERMINAL SARAF-BASED PEPTIDES AS MODULATORS OF THE SOCE RESPONSE.

To evaluate the effect of C-terminal SARAF protein overexpression in SOCE response, we recorded calcium imaging using Fura-2 AM in MDA-MB-231 cells and 4T1 cells. The SOCE protocol described in the materials and methods section was applied. We observed a decreased Ca^{2+} entry when mScarlet-C-SARAF and mScarlet-C-SARAF^{K326R} were overexpressed in both human MDA-MB-231 (Figure 3) and murine 4T1 (Figure 4) TNBC cells line in comparison to the control. This result is consistent with the effects reported by Palty *et al*. (2012), observing the reduction of the SOCE response dependent on SARAF protein determined by the C-terminal regionv[71]. However, no significant differences were observed between C-SARAF fragments wild-type and mutant in both cell lines (Figures 3 and 4).

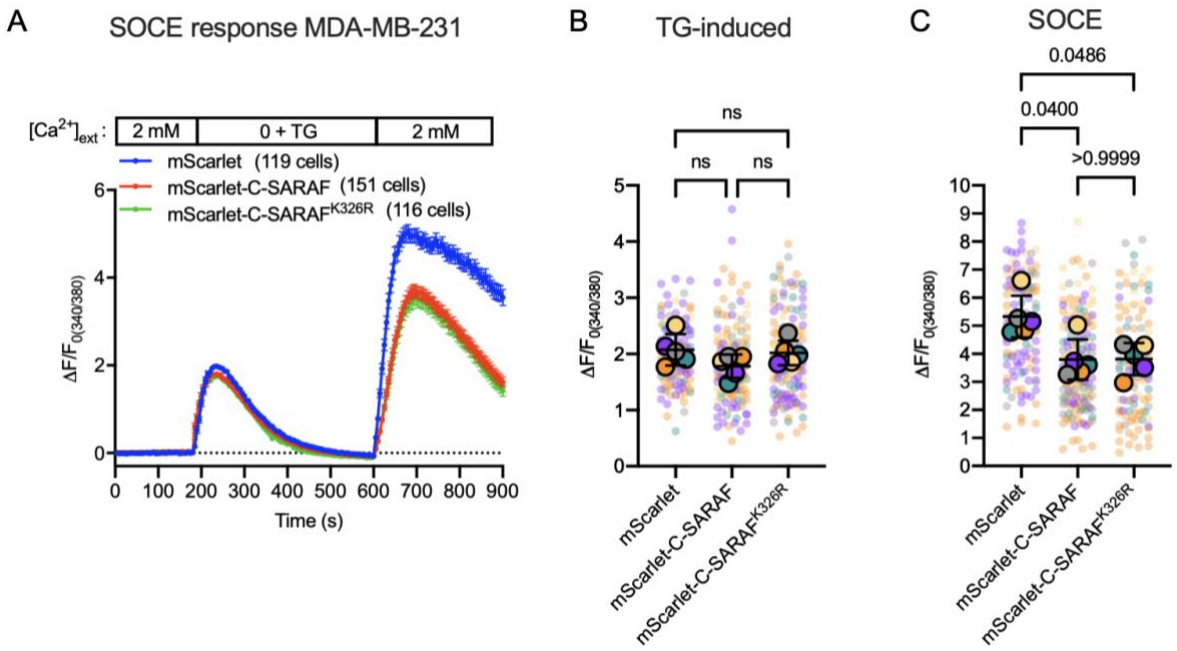

Figure 3. mScarlet-C-SARAF fragments decrease the SOCE response in the human TNBC cell line.

A Representative graph of SOCE response. mScarlet-C-SARAF and mScarlet-C-SARAF^{K326R} were overexpressed in MDA-MB-231 cells which were loaded with Fura-2 AM and then calcium imaging was performed. The protocol used consisted of 3 minutes with Ringer's solution of 2 mM $CaCl_2$, then Ca^{2+} depletion was induced with Calcium free-Ringer's solution with 1 mM EGTA and 2 µM of thapsigargin (TG) for 7 minutes. Finally, the solution is changed to Ringer's 2 mM $CaCl_2$ to induce calcium entry. **B-C.** Representative graph of maximum peak TG-induced and maximum Ca^{2+} influx in MDA-MB-231 SOCE response respectively. Each independent experiment is represented with color and expressed as individual data per cell and as average per experiment (n=5). Statistical analysis used in graphs B and C was One-way ANOVA Dunn's multiple comparisons test.

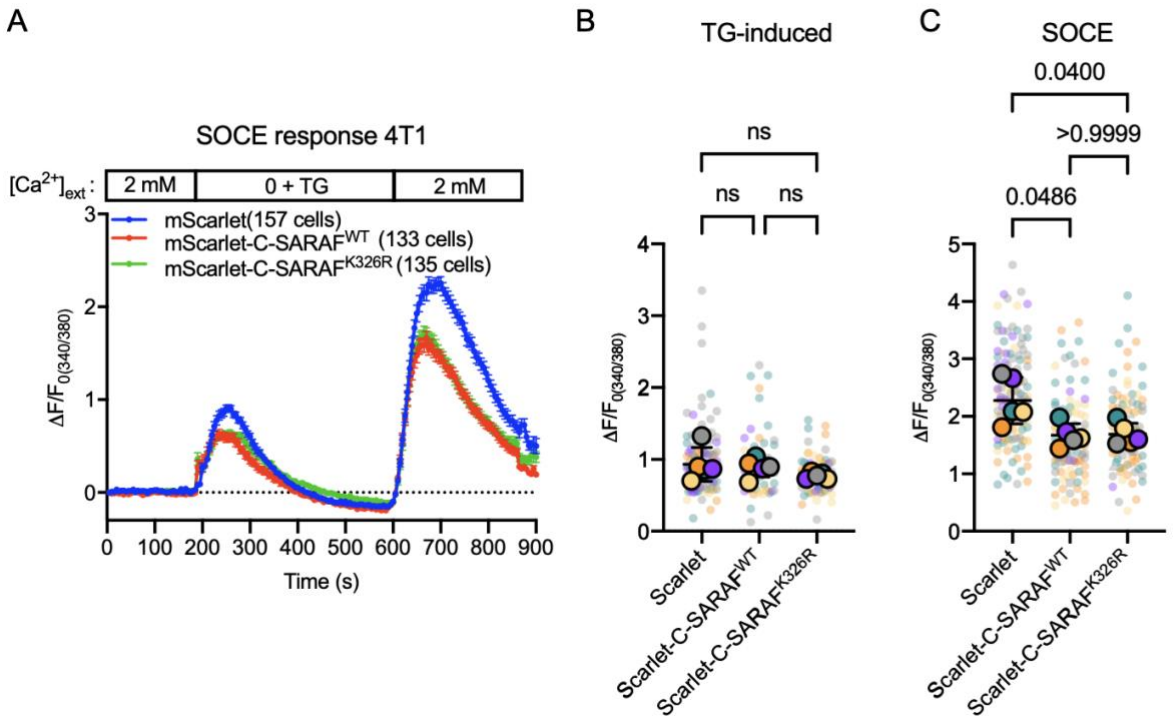

Figure 4. mScarlet-C-SARAF fragments decrease the SOCE response in murine TNBC cell line.

A Representative graph of SOCE response. mScarlet-C-SARAF and mScarlet-C-SARAF^{K326R} were overexpressed in 4T1 cells which were loaded with Fura-2 AM and then calcium imaging was performed. The protocol used consisted of 3 minutes with Ringer's solution of 2 mM $CaCl_2$, then Ca^{2+} depletion was induced with Calcium free-Ringer's solution with 1 mM EGTA and 2 µM of thapsigargin (TG) for 7 minutes. Finally, the solution is changed to Ringer's 2 mM $CaCl_2$ to induce calcium entry. **B-C** Representative graph of maximum peak TG-induced and maximum Ca^{2+} influx in 4T1 SOCE response respectively. Each independent experiment is represented with color and expressed as individual data per cell and as average per experiment (n=5). Statistical analysis used in graphs B and C was One-way ANOVA Dunn's multiple comparisons test.

The C-terminal of SARAF is required for the interaction with STIM1[71]. Considering the effect of the C-terminal fragment of SARAF onto SOCE (Figure 3 and 4), we evaluated the formation of the STIM1 cluster in MDA-MB-231 cells that overexpress the plasmids STIM1-YFP and mScarlet, mScarlet-C-SARAF or mScarlet-C-SARAF^{K326R}. STIM1 cluster formation was induced after reticular Ca^{2+} depletion using thapsigargin. We did not observe significant differences between the control condition and the overexpression of mScarlet-C-SARAF (Figure 5). However, the overexpression of the mScarlet-C-SARAF^{K326R} fragment presents a slower rate of the

kinetics of STIM1 cluster formation or slows down the translocation of these, which could affect the timing of signaling.

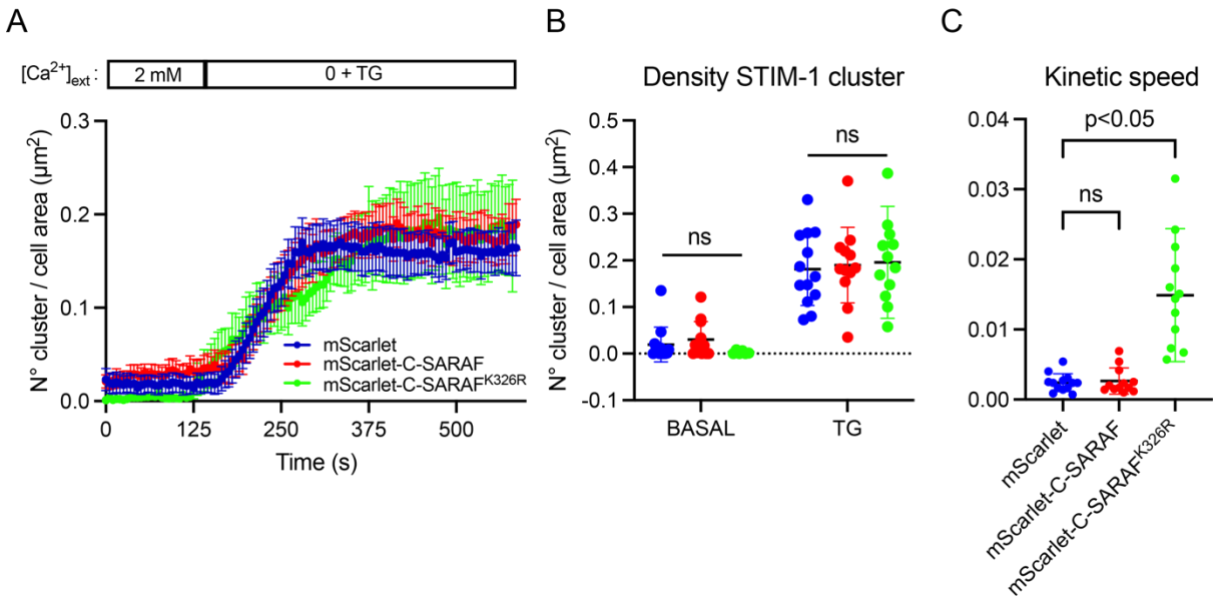

Figure 5. mScarlet-C-SARAF^{K326R} decreases the kinetic rate of STIM1 cluster formation in the human TNBC cell line.
A Graph showing the kinetics of STIM cluster formation in MDA-MB-231 cells that overexpress mScarlet, mScarlet-C-SARAF, or mScarlet-C-SARAF^{K326R}. **B** Graph of the quantification of cluster density. **C** Graph of the quantification of kinetic rate. Seven independent experiments were performed. Statistical analysis used in graphs B and C was One-way ANOVA Dunn's multiple comparisons test.

Given that the C-terminal fragment of SARAF reduces SOCE response, we evaluated whether affects the formation of the STIM1-Orai1 complex, which is a key event for the activation of the response [42–44,50,104] . We used a Bimolecular fluorescence complementation (BiFC) assay to directly visualize protein-protein interaction *in vivo* using fixed cells. The fluorescence signal is reconstituted by complementing two fragments of the fluorescent protein Venus (Venus-N, and Venus-C[105]). Therefore, MDA-MB-231 and 4T1 cells were co-transfected with mScarlet, mScarlet-C-SARAF, or mScarlet-C-SARAF^{K326R} and with STIM1-VC and Orai1-VN and STIM1/Orai1 complementation[106] was stimulated by addition of 2 µM TG in Ringer's solution modified 2 mM $CaCl_2$. We observed that the overexpression of the fragments reduces the formation of the STIM1-Orai1 complex in human and murine TNBC cells line (Figure 6 y 7), which supports the effect observed with the calcium recordings (Figure 3 and 4).

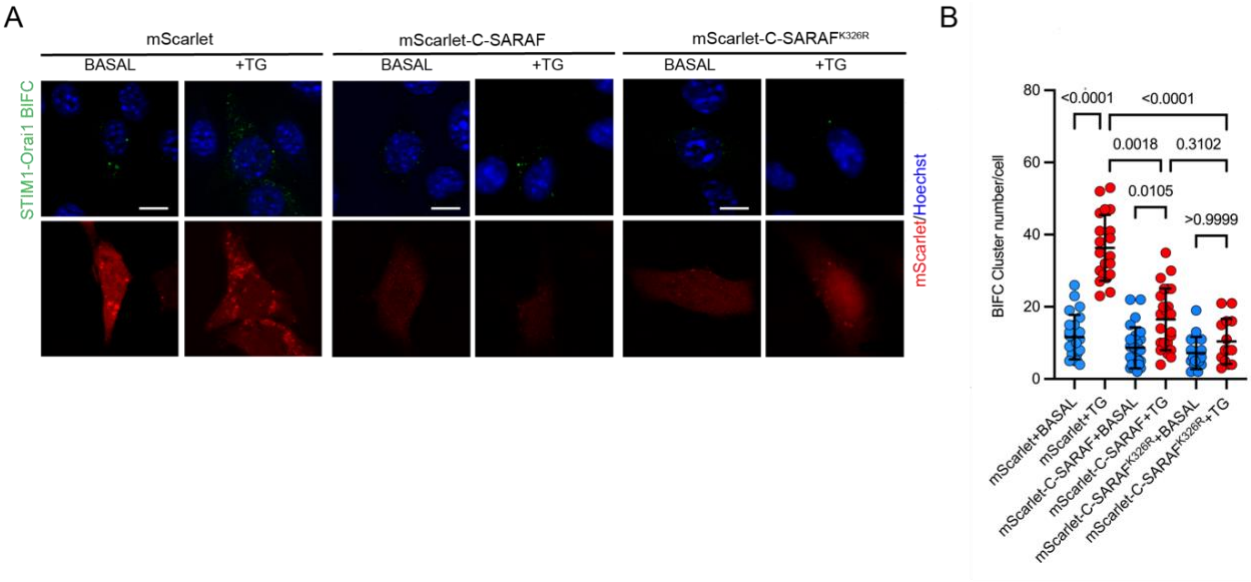

Figure 6. mScarlet-C-SARAF fragments decrease the formation of the STIM1-ORAI complex in the human TNBC cell line.

A Representative images of BiFC STIM1-Orai in MDA-MB-231 cells that overexpressed mScarlet, mScarlet-C-SARAF, or mScarlet-C-SARAF^{K326R}. Blue corresponds to the nucleus of the cell, red corresponds to the expression of the proteins tagged with mScarlet and green dots correspond to the conformation of the STIM1-Orai1 complex. **B** Graphs of the quantification of cluster numbers per cell corresponding to BiFC of STIM1-Orai1. Three independent experiments were performed on each cell line. The statistical analysis used was One-way ANOVA Dunn's multiple comparisons test. Scale bar= 20 μm.

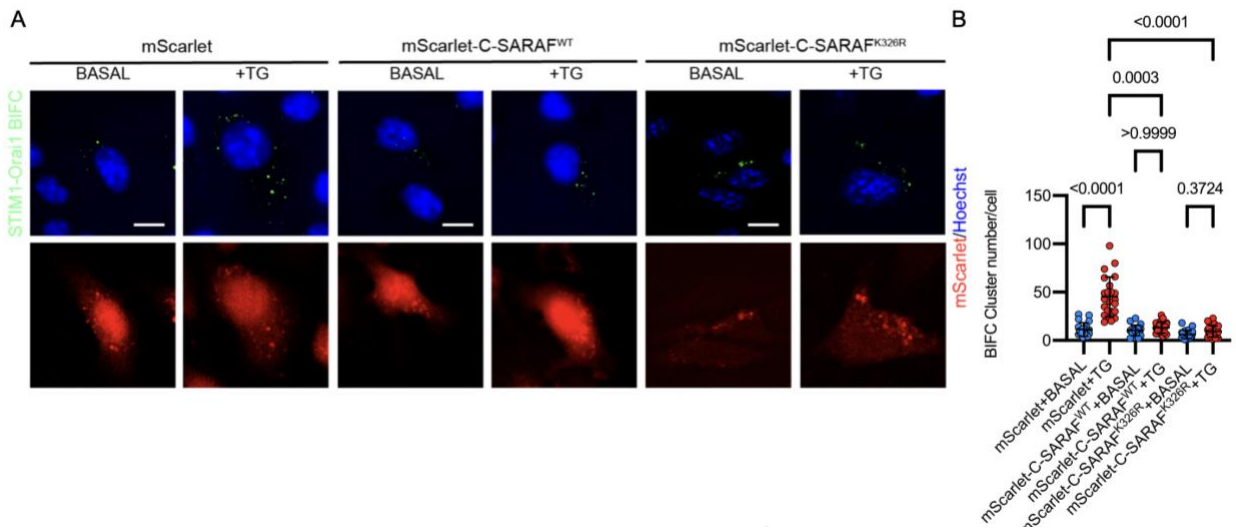

Figure 7. mScarlet-C-SARAF fragments decrease the formation of the STIM1-ORAI complex in the murine TNBC cell line.

A Representative images of BiFC STIM1-Orai in 4T1 cells that overexpress mScarlet, mScarlet-C-SARAF, or mScarlet-C-SARAF^{K326R}. Blue corresponds to the nucleus of the cell, red corresponds to the expression of the proteins tagged with mScarlet and green dots correspond to the conformation of the STIM1/Orai1 complex. **B** Graphs of the quantification of cluster numbers corresponding to BiFC of STIM1-Orai. Three independent experiments were

performed on each cell line. The statistical analysis used was One-way ANOVA Dunn's multiple comparisons test. Scale bar= 20 μm.

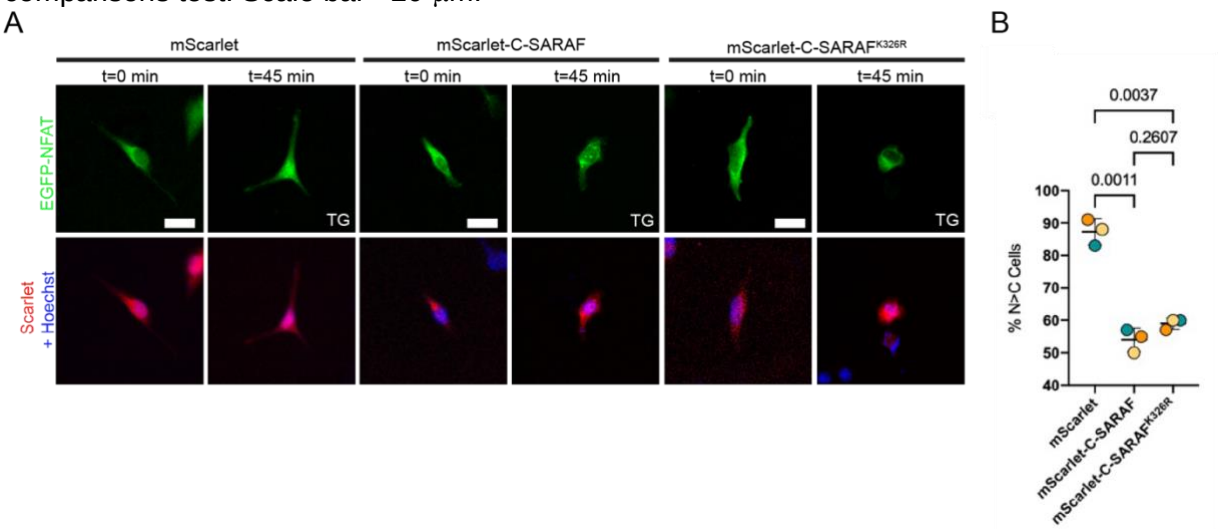

Figure 8. mScarlet-C-SARAF fragments reduce NFAT1 activity in human TNBC cells line.
A Representatives images of the translocation of NFAT from the cytoplasm to the nucleus in MDA-MB-231 cells. **B** Graph of the quantification of translocation of NFAT from cytoplasm to the nucleus. Three independent experiments were performed. Scale bar= 20 μm..

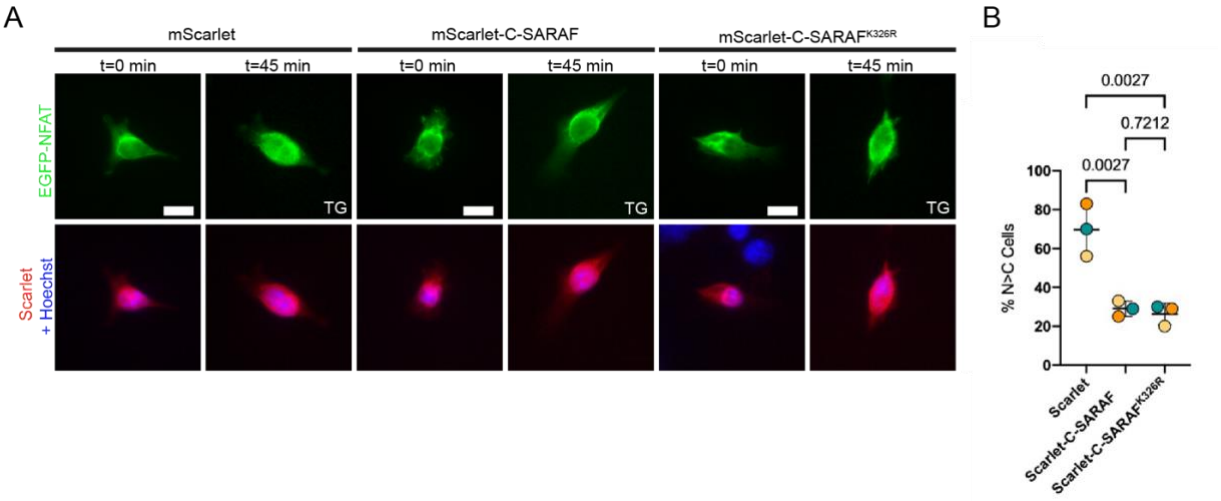

Figure 9. mScarlet-C-SARAF fragments reduce NFAT1 activity in murine TNBC cell line.
A Representatives images of the translocation of NFAT from the cytoplasm to the nucleus in 4T1 cells. **B** Graph of the quantification of translocation of NFAT from cytoplasm to the nucleus. Three independent experiments were performed. Scale bar= 20 μm.

Finally, we evaluated the activation of signaling downstream of the activation of SOCE response such as NFAT[107]. The family of transcription factors known as the nuclear factor of activated T cells (NFAT) consists of four members (NFAT1-4) that are

regulated by calcium and one member (NFAT5) that is regulated in response to osmotic stress. Normally, NFAT1-4 proteins are in the cytoplasm in a hyperphosphorylated form when cells are unstimulated. However, when cell surface receptors are activated and calcium is released from intracellular stores, calcium-dependent enzymes are activated, particularly the calcineurin (Cn) protein phosphatase. Cn catalyzes the dephosphorylation of NFAT, causing it to move into the nucleus where it regulates gene transcription[108]. In the context of triple-negative breast cancer, Quang *et al.* (2015) determined that NFAT1 and NFAT2 are key in the migration and invasion processes of 4T1 cells[109]. Based on this, the translocation of EGFP-NFAT from the cytoplasm to the nucleus was observed in MDA-MB-231 and 4T1 cells stimulated by the addition of 2 µM TG in Ringer's solution-modified 2 mM $CaCl_2$. The data obtained suggest a reduction of NFAT translocation when mScarlet-C-SARAF fragments were overexpressed in both cell lines (Figures 8 and 9) which suggests that both fragments, in addition to having a negative effect on the SOCE response, could affect the migratory and invasive phenotype of tumor cells.

AIM 2. DETERMINE THE EFFECT OF THE C-TERMINAL SARAF-BASED PEPTIDES DURING CELL MIGRATION AND INVASION IN *IN VITRO* MODEL OF TRIPLE-NEGATIVE BREAST CANCER.

Given that the SOCE response has been related as a key signaling mechanism in the regulation of migration and invasion of cancer tumor cells, among other mechanisms[110], the overexpression of mScarlet-C-SARAF in tumor cells could also affect this process. It is in this context that we performed an MTT assay to evaluate cell proliferation. No effects on proliferation were observed in MDA-MB-231 and 4T1 cells after overexpression of mScarlet-C-SARAF fragments (Figure 10).

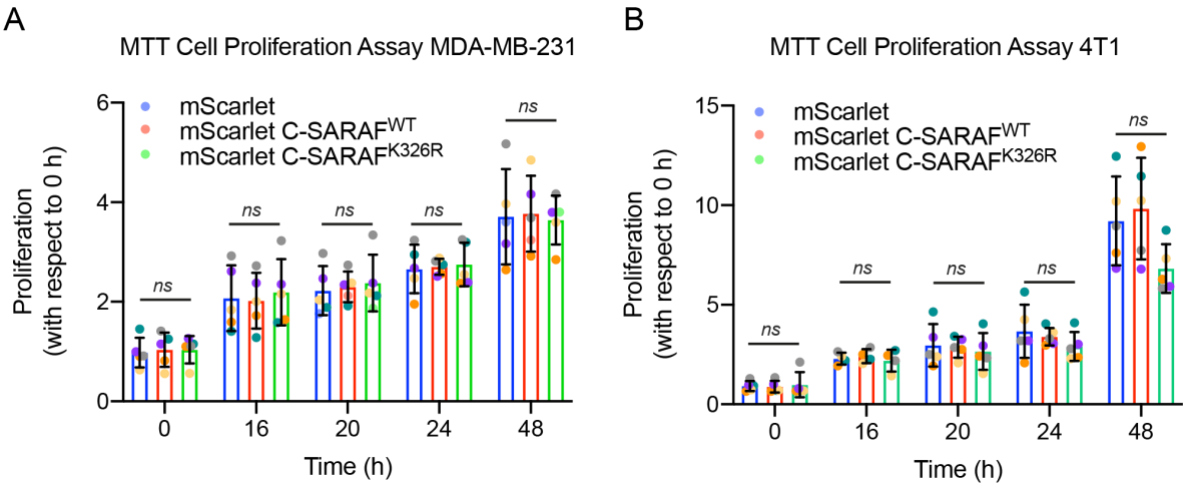

Figure 10. mScarlet-C-SARAF fragments does not affect cell proliferation.
A-B. Representative graph in the rate of proliferation in human and murine TNBC cell line respectively, after overexpression of mScarlet, C-SARAF, and C-SARAF^{K326R} evaluated with MTT assay. Each dot represents an independent experiment. Each assay corresponds to N=5. The statistical analysis used was One-way ANOVA Dunn's multiple comparisons test.

Cell migration and invasion cell assay were performed. First, we observed a decrease in collective migration in both MDA-MB-231 and 4T1 cells (Figures 11 and 12) when we overexpressed the mScarlet-C-SARAF and mScarlet-C-SARAF^{K326R} fragments compared to the control. We did not observe significant differences between the mScarlet-C-SARAF and mScarlet-C-SARAF^{K326R} conditions, but a greater effect on the reduction of migration in the mScarlet-C-SARAF mutant condition. Therefore, the data suggest that mScarlet-C-SARAF and mScarlet-C-SARAF^{K326R} reduce the SOCE response in TNBC. However, only mScarlet-C-SARAF^{K326R} could have an effective effect in decreasing cell migration in MDA-MB-231 and 4T1.

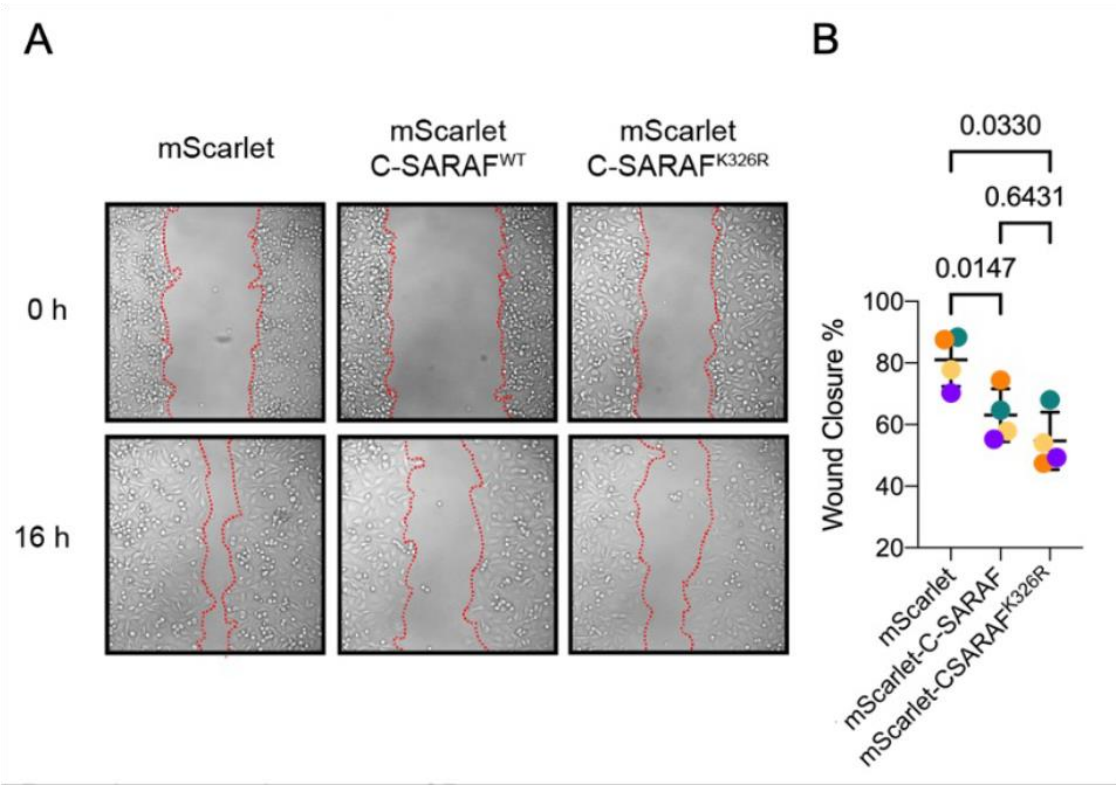

Figure 11. mScarlet-C-SARAF fragments decrease cell migration in human TNBC cells line.

A Representative image of Scratch assay after overexpression of mScarlet-C-SARAF and mScarlet-C-SARAF^{K326R} in MDA-MB-231 cells line. **B** Representative graph of the quantification of wound closure area of four independent experiments performed in MDA-MB-231. The statistical analysis used was One-way ANOVA Dunn's multiple comparisons test.

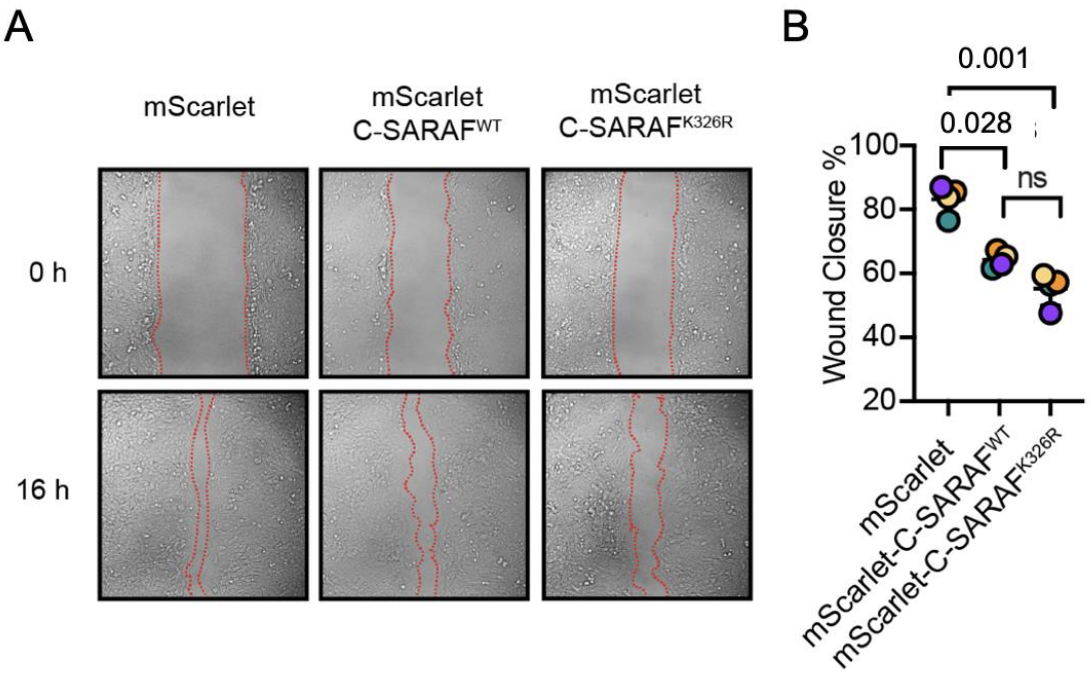

Figure 12. mScarlet-C-SARAF fragments decrease cell migration in the murine TNBC cell line.

A Representative images of Scratch assay after overexpression of mScarlet-C-SARAF and mScarlet-C-SARAF^{K326R} in 4T1 cells line. **B** Representative graph of the quantification of wound closure area of four independent experiments performed in 4T1. The statistical analysis used was One-way ANOVA Dunn's multiple comparisons test.

As previously mentioned, cell invasion is key in the highly metastatic phenotype of TNBC[87]. We performed invasion assays in a transwell chamber with MDA-MB-231 cells and 4T1 cells. The data suggest a reduction in the migration of cells that overexpress mScarlet-C-SARAF and mutant in both human and murine TNBC cells (Figures 13 and 14).

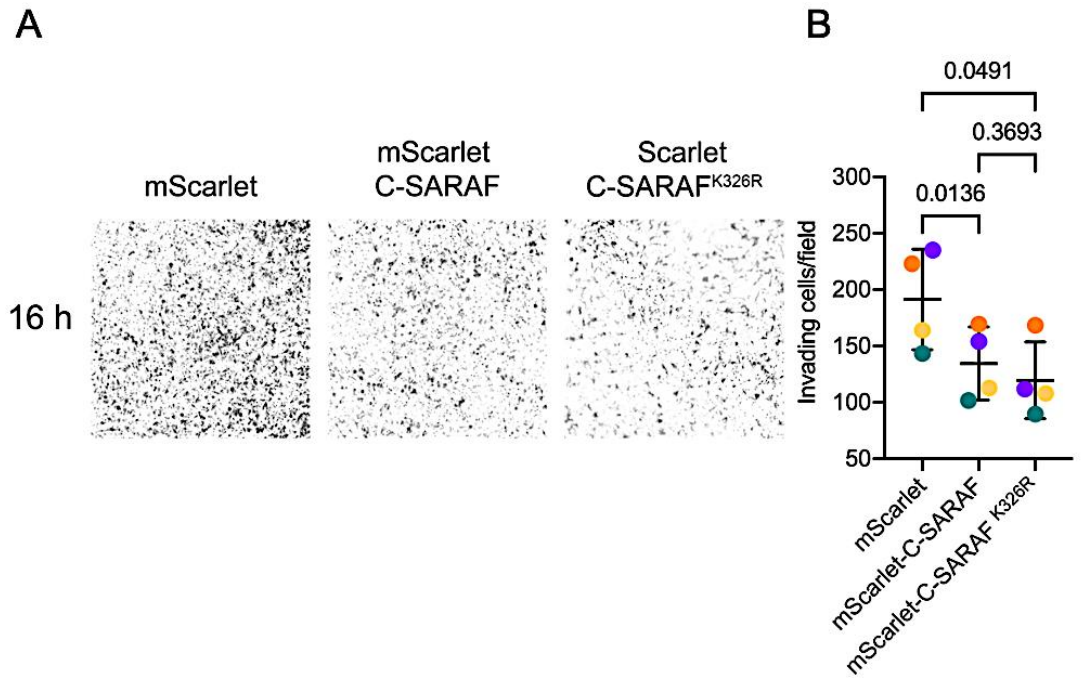

Figure 13. mScarlet-C-SARAF fragments decrease the invasion in the human TNBC cell line.

A Representatives images of Transwell cell invasion assay in MDA-MB-231 cells overexpressing mScarlet, mScarlet-C-SARAF, and mScarlet-C-SARAF^{K326R}. **B**. Representative graph of the quantification of invading cells in four independent experiments performed. The statistical analysis used was One-way ANOVA Dunn's multiple comparisons test.

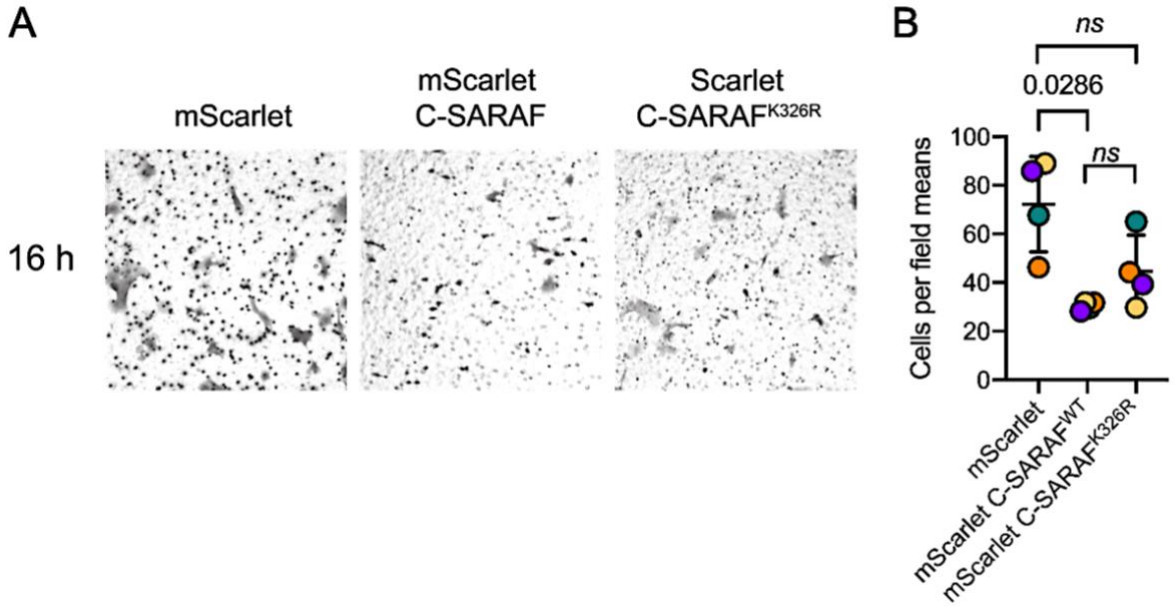

Figure 14. mScarlet-C-SARAF fragments decrease the invasion in the murine TNBC cell line.

A Representatives images of Transwell cell invasion assay in 4T1 cells overexpressing mScarlet, mScarlet-C-SARAF, and mScarlet-C-SARAF^{K326R}. **B** Representative graph of the

quantification of invading cells per field in four independent experiments performed. The statistical analysis used was One-way ANOVA Dunn's multiple comparisons test.

Another relevant cellular process in cell migration and invasion is the formation of focal adhesions and actin dynamics provide the main sites of cell adhesion to the extracellular matrix and associate with the actin cytoskeleton to control cell movement [111]. In this sense, we performed cell spreading assays in MDA-MB-231 (Figure 15) cells and 4T1 (Figure 16). We observed that the overexpression of mScarlet-C-SARAF fragments reduces the extension of the adhered cells compared to the control in MDA-MB-231 cells, (Figure 15). The mScarlet-C-SARAF fragment expression did not show significant differences (Figure 16) in 4T1 cells.

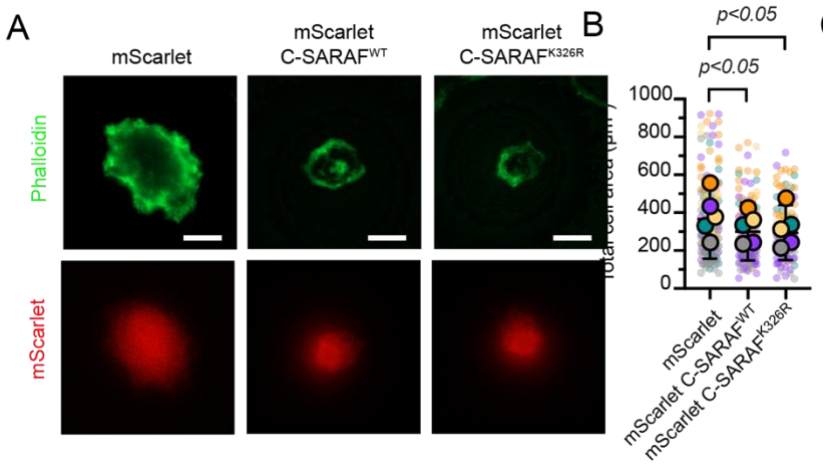

Figure 15. mScarlet-C-SARAF fragments reduce the cell spreading in the human TNBC cell line.

A Representative immunofluorescence panels of the effect of mScarlet, mScarlet-C-SARAF, or mScarlet-C-SARAF^{K326R} overexpression in MDA-MB-231 on cell spreading. **B** Graph of Total area cell from MDA-MB-231 cells. Five independent experiments were performed. The statistical analysis used was One-way ANOVA Dunn's multiple comparisons test. Scale bar= 20 μm.

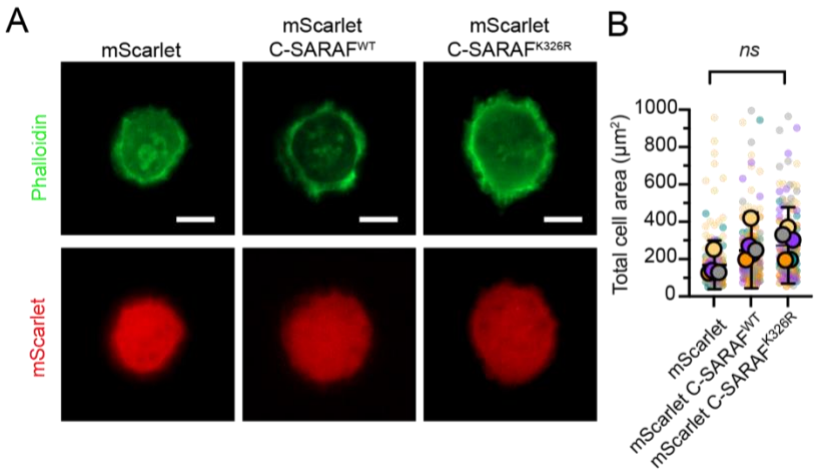

Figure 16. mScarlet-C-SARAF fragments does not affect the cell spreading in the murine TNBC cell line.
A Representative immunofluorescence panels of the effect of mScarlet, mScarlet-C-SARAF, or mScarlet-C-SARAF^{K326R} overexpression in 4T1 cells on cell spreading. **B** Graph of Total area cell. Five independent experiments were performed. The statistical analysis used was One-way ANOVA Dunn's multiple comparisons test. Scale bar= 20 µm.

In addition, we performed focal adhesion dynamics assays using TIRF microscopy, by recording the fluorescence intensity of the EGFP-Paxillin protein[93] (Figure 17). We evaluated the assembly and disassembly rate of focal adhesions in MDA-MB-231 cells when overexpressing mScarlet-C-SARAF fragments. The data suggest that mScarlet-C-SARAF fragment increases the rate of assembly, while mScarlet-C-SARAF^{K326R} reduces their disassembly (Figure 17 B-C). Moreover, we evaluated the area of the cell that protrudes and retracts (Figure 18). We observed that the overexpression of both fragments reduced this area in comparison with the control, which suggests that the fragments could affect the rearrangement dynamics of the actin cytoskeleton, which would support the effect observed in the spreading assay (Figure 15).

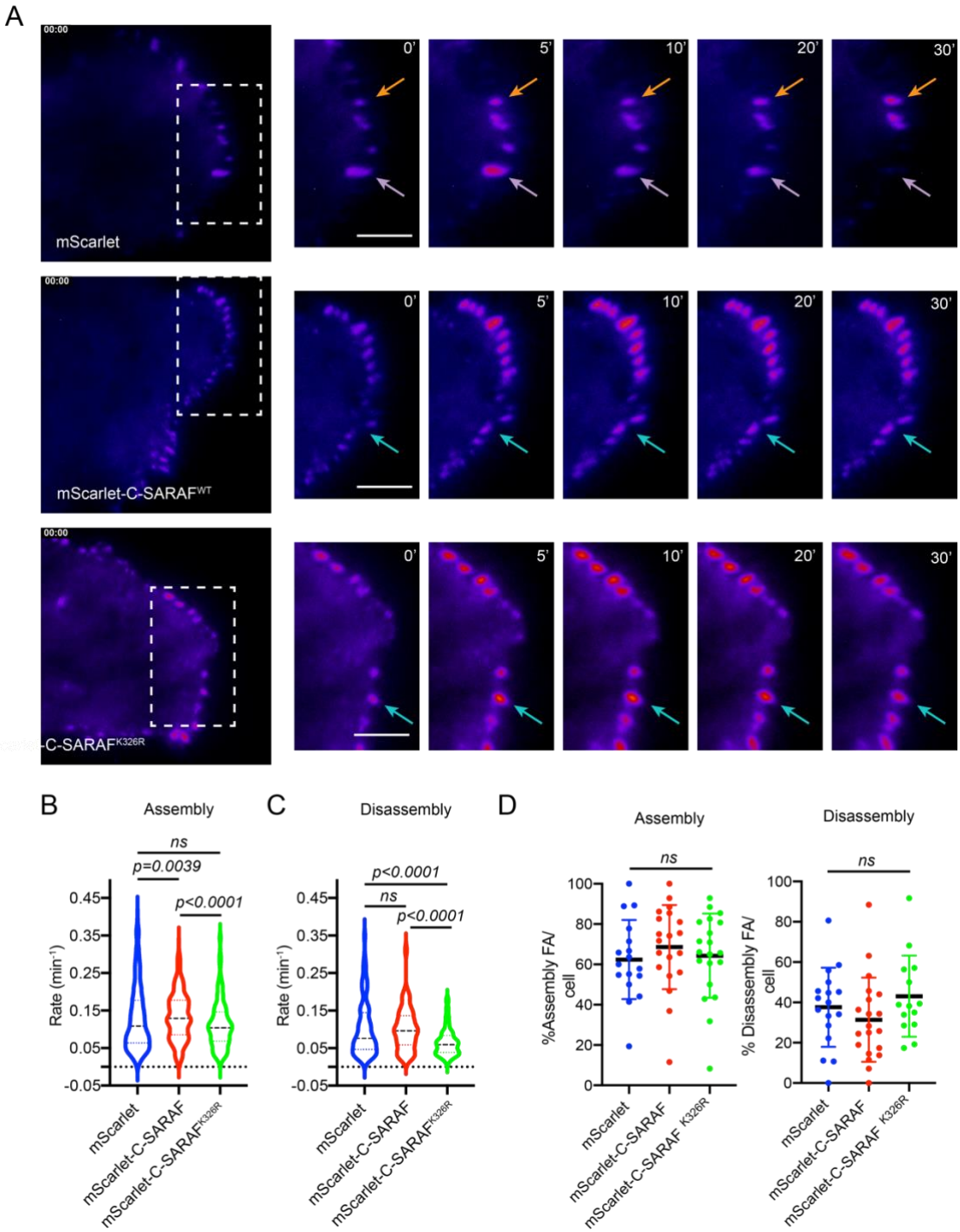

Figure 17. mScarlet-C-SARAF fragments reduce disassembly focal adhesion in human TNBC cell line.

A Representative image panels of the effect of mScarlet, mScarlet-C-SARAF, or mScarlet-C-SARAF^{K326R} overexpression in MDA-MB-231 on focal adhesions dynamic. **B** Graph of Assembly rate of focal adhesion. **C** Graph of Disassembly rate of focal adhesion. **D** Graph of pattern of focal adhesion dynamics. 21 cells were analyzed. Scale bar= 5 μm. The statistical analysis used was One-way ANOVA Dunn's test.

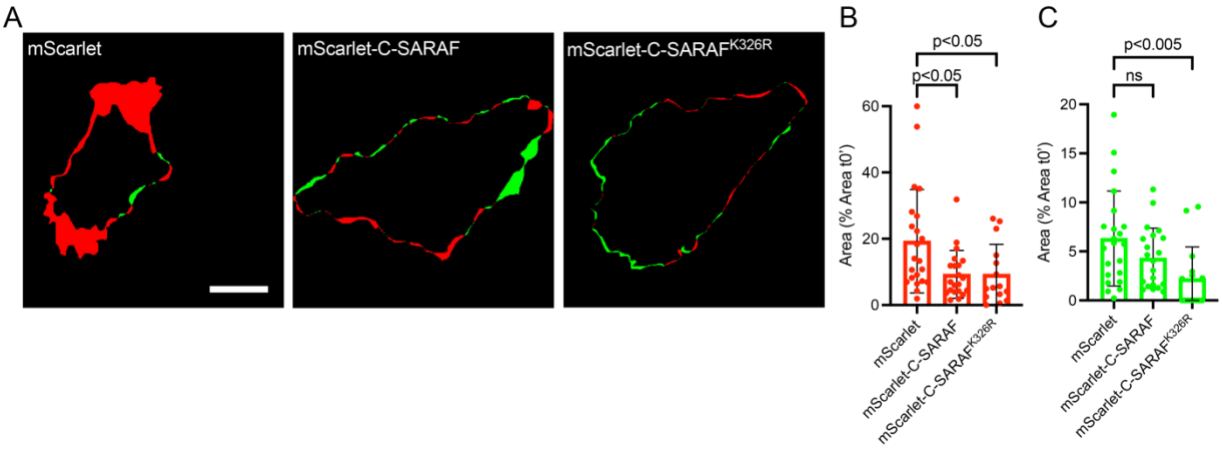

Figure 18. mScarlet-C-SARAF fragments reduce protrusion and retraction process in human TNBC cell line.
A Representative image panel of the effect of mScarlet, mScarlet-C-SARAF, or mScarlet-C-SARAF^{K326R} overexpression in MDA-MB-231 on protrusion (red area) and retraction cell (green area). **B** Graph of % area of protrusion and retraction when cells were stimulated with 10%FBS during focal adhesion dynamics analyses (Figure 17). Scale bar= 20 μm. The statistical analysis used was One-way ANOVA Dunn's test.

Together, these data suggest that the expression of mScarlet-C-SARAF fragments could contribute to the reduction of cell migration and invasion by altering the formation of focal adhesions and actin polymerization.

AIM 3. DETERMINE THE EFFECT OF THE C-TERMINAL SARAF-BASED PEPTIDES IN THE MURINE *IN VIVO* MODEL OF TRIPLE-NEGATIVE BREAST CANCER.

Based on the data suggesting a reduction in migration and invasion in TNBC cells when we overexpress mScarlet-C-SARAF fragments above all the mutant version and the relevance of the tumor microenvironment on neoplastic cells we performed a tumor growth assay in an *in vivo* murine model. For this, we injected 4T1 cells that overexpress mScarlet, mScarlet-C-SARAF, and mScarlet-C-SARAF^{K326R} in the fourth inguinal gland. After approximately 21 days, the mice were euthanized (Figure 19). According to the volumes of the primary tumors obtained, no significant differences were observed between the conditions (Figure 20). This suggests that the mScarlet-C-SARAF fragments do not affect the proliferation of neoplastic cells *in vitro* (Figure 10) and *in vivo*.

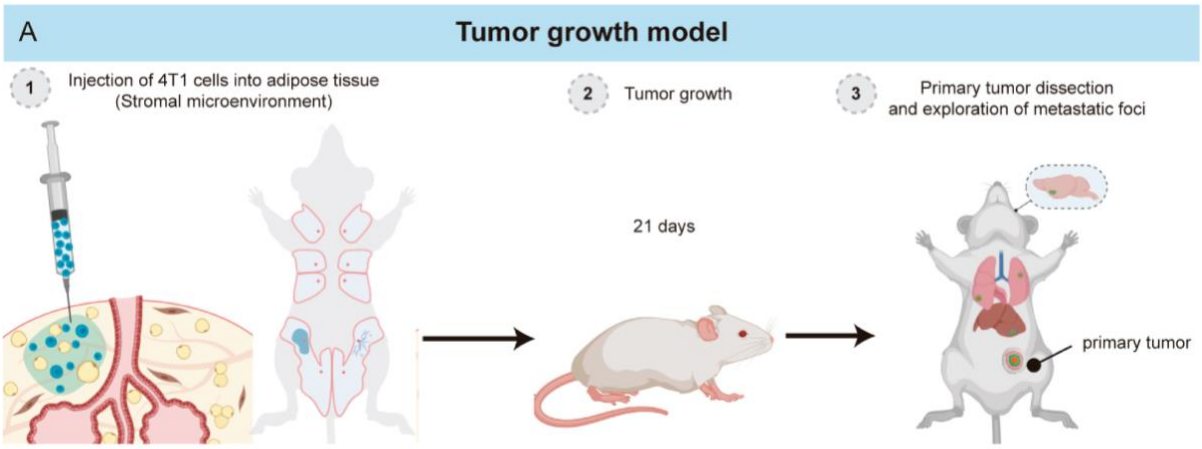

Figure 19. Diagram of murine *in vivo* tumor growth model.
A1 represents an orthologous injection of 4T1 cells stably overexpressing the mScarlet, mScarlet-C-SARAF, or mScarlet-C-SARAF^{K326R} fragments into adipose tissue pad present in the fourth inguinal mammary gland. Then mice are monitored for 21 days (A2) to finally apply euthanasia and perform a necropsy (A3).

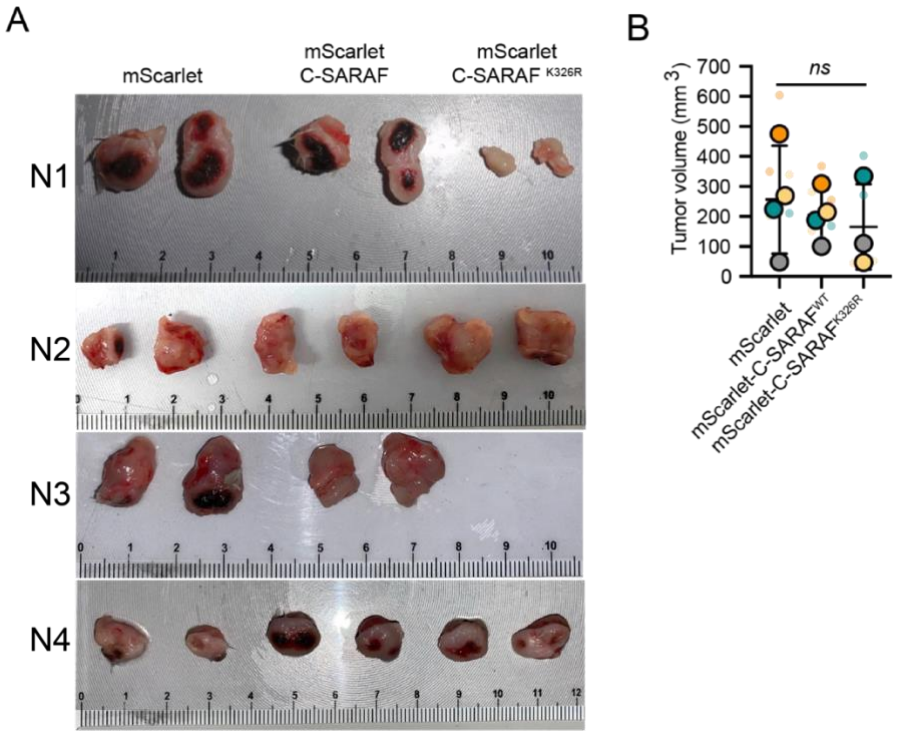

Figure 20. mScarlet-C-SARAF fragments do not affect the primary tumor growth of TNBC *in vivo* model.
A Images of primary tumors obtained after injection of stable lines of 4T1 overexpressing mScarlet, mScarlet-C-SARAF, or mScarlet-C-SARAF^{K326R} in the fourth mammary gland of Balb/c mice. **B** Graph of primary tumor volume. The statistical analysis used was One-way ANOVA Dunn's test.

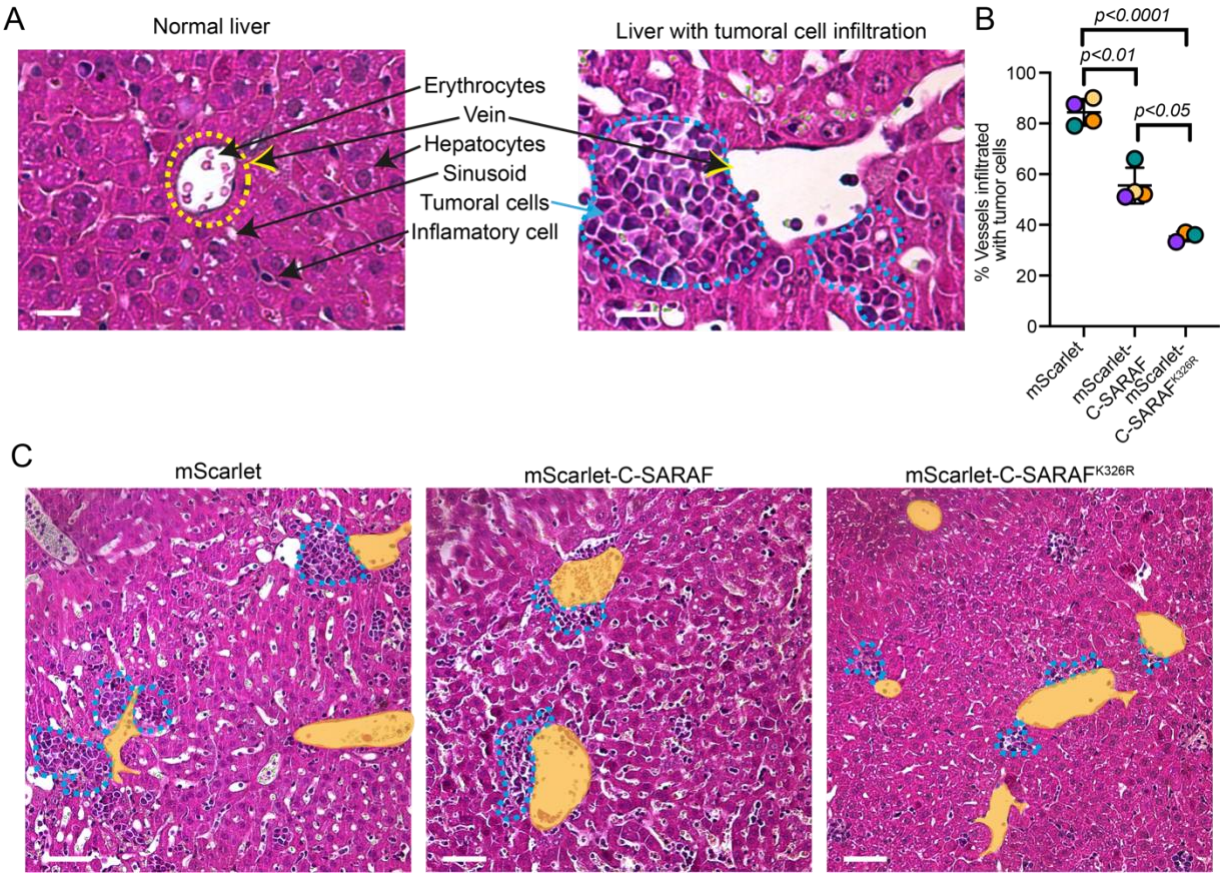

Figure 21. mScarlet-C-SARAF fragments reduce metastasis in the liver of primary tumor growth TNBC *in vivo* model.

A Representative image of histological sections of liver samples with Hematoxylin and eosin, magnification 20X. Scale bar= 50 μm. **A** Representative image of normal and infiltrated liver histology, highlighting the different structures observed in the mouse samples for the development of the tumor growth model. **B** Graph shows quantification of the percentage of vessels present in the liver infiltrated with tumor cells. The statistical analysis used was One-way ANOVA Brown-Forsythe and Welch test. **C** Representative images of samples stained with hematoxylin and eosin at 20X magnification. Scale bar= 150 μm. The yellow zone shows the luminal vein of liver tissue and areas delimited with light blue dashed lines show tumor cells that infiltrate the vein. The statistical analysis used was One-way ANOVA Brown-Forsythe and Welch test.

Next, then we analyze the possible organs that could be affected by metastatic foci of the primary tumor. In TNBC, the liver, brain, and lung are the main organs affected. We analyzed areas of tumoral cells infiltrated in the histological section of the liver stained with hematoxylin and eosin. Interestingly, we observed the presence of neoplastic cells in the liver parenchyma, mainly infiltrating the vessels (Figure 21). We show that the overexpression of the mScarlet-C-SARAF fragments reduces the infiltration of neoplastic cells in the tumor, which suggests that the overexpression of

mScarlet-C-SARAF fragments reduces the metastatic capacity of tumor cells that constitute the primary tumor which supports the effect observed in *in vitro* migration and invasion assays. In addition, using Masson's trichrome staining (Figure 22) we observed that tumor cells that constitute the primary tumor are accompanied by a large inflammatory infiltrate (TIL). TILs can be measured in slides stained with hematoxylin and eosin, presenting variation in density and location in the tumor[11,102]. TILs are reported as area occupied by mononuclear inflammatory cells over total intratumoral stromal area, where all mononuclear cells (including lymphocytes and plasma cells) should be scored, but polymorphonuclear leukocytes are excluded[102].

We observed a greater area of infiltrating lymphocyte cells in the primary tumor of the mScarlet-C-SARAF^{K326R} condition compared to the control which suggests that the overexpression of mScarlet-C-SARAF^{K326R} could have a lower tumor growth given that the tumor microenvironment allows the inflammatory system to act against cancer progression, being also an indication of being a sensitizer of the primary tumor to conventional therapies used allowing a better forecast.

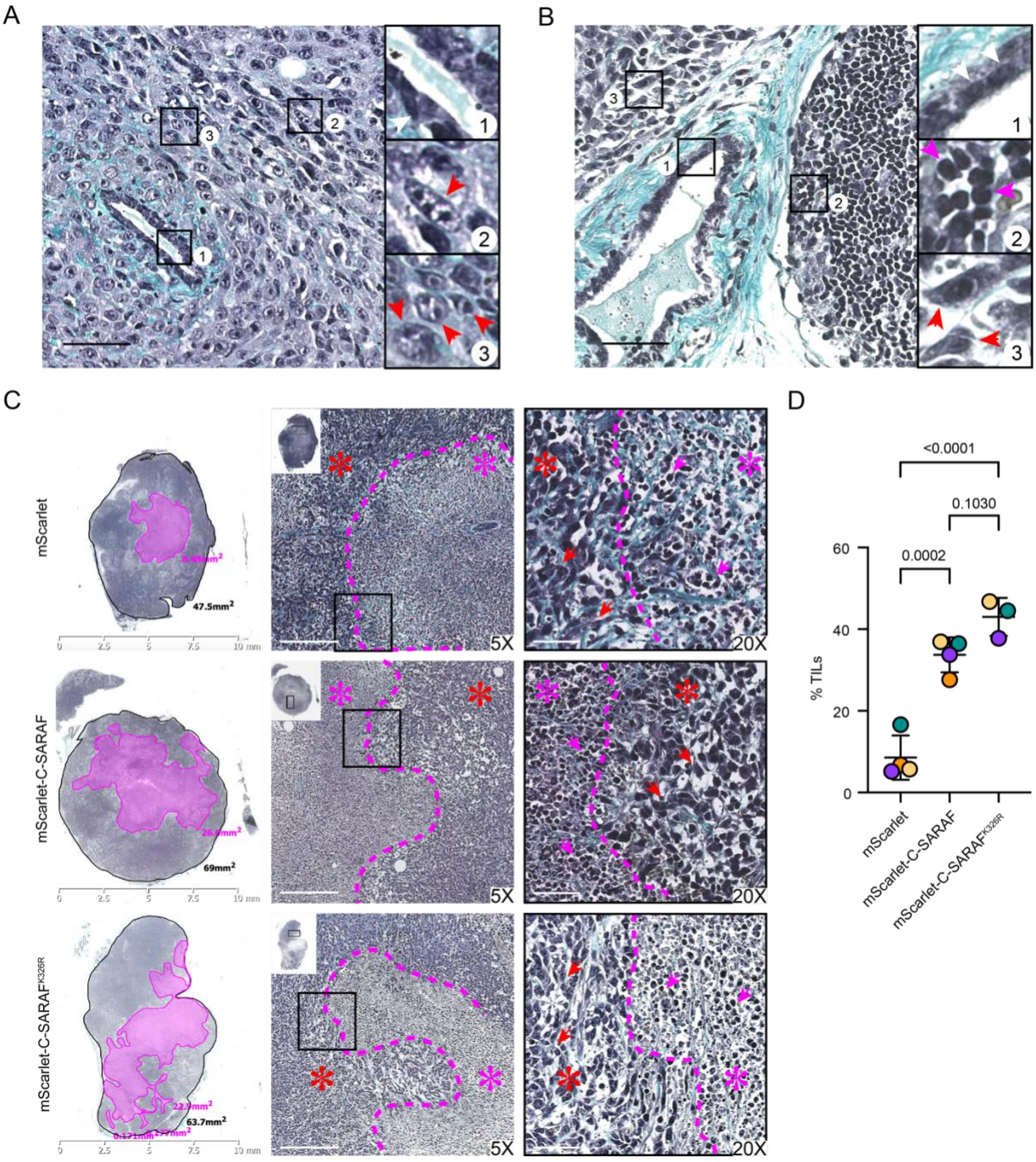

Figure 22. mScarlet-C-SARAF fragment increase lymphocyte infiltration in primary tumor growth of TNBC *in vivo* model.

Representative images of histological sections of the primary tumor of the animal model stained with Masson's trichrome. **A** 20X image shows tumor cells present in the stroma and surrounding normal mammary epithelium. Scale bar= 50 μm. Insets 1-3 are 63X images of **A** numbered black boxes. **Inset 1** shows mammary duct structure with normal epithelial cells. White arrow indicates purple nuclei with uniform nuclear chromatin and palisade distribution consistent with normal histology. **Inset 2**, red arrow shows chromatin alteration with the presence of 3 nucleoli. **Inset 3**, red arrows show chromatin-altered nuclei with different numbers of nucleoli and irregular sizes and shape. **B** 20X image shows tumor cells present in

the breast tissue stroma, normal breast epithelial tissue surrounded by collagen (light green color), as well as a cluster of inflammatory infiltrates. Scale bar= 50 μm. Insets 1-3 are 63X images of numbered black box image in **B**. **Inset 1**, shows mammary duct structure with normal epithelial cells. White arrows indicate purple nuclei with homogeneous staining and palisade distribution consistent with normal histology. **Inset 2**, fuchsia arrows indicate small lymphocytes with similar size, spherical heterochromatic nuclei, and scant cytoplasm. **Inset 3**, red arrows show neoplastic cell nuclei of fused morphology that present condensed nuclei of different shapes and sizes. **C** corresponds to a panel of histological samples scanned and visualized with the NDP program at 0.38X, 5X and 20X magnification. Lower magnification images show visualization of the complete histological section of the primary tumor of each condition, in black indicates the total area of the neoplastic tissue. Fuchsia region corresponds to the total area of inflammatory infiltrate present in the tumor. 5X and 20X images show representative areas in which an area of inflammatory infiltrate is observed (segmented by a fuchsia dashed line and indicated by the asterisk of the same color) and tumor tissue (indicated by the red asterisk). Red arrows indicate neoplastic cells that present nuclear atypia also evidenced in **A** and **B**. Fuchsia arrows indicate lymphocytes with cell morphology consistent with that evidenced in **B**. Scale bar= 100 μm for 5X images and Scale bar= 10 μm for 20X images. **D** Graph shows percentage of inflammatory infiltrate present in histological sections of primary tumor. Statistical analysis used was One-way ANOVA Dunn's test.

DISCUSSION

Calcium signaling is a crucial component in several processes. A dysregulation of calcium signaling has been observed in breast cancer, affecting tumorigenesis and different cellular processes, such as cell growth and proliferation, migration, metastasis, and resistance to apoptosis. Interestingly, an increased expression of molecular components of the SOCE response has been reported, such as an increase in the expression of ORAI channels[39,124], TRPC1[125,126], TRPC6[127–129], STIM [87,130–132] proteins, among others. However, only a few regulators of the SOCE response involved in this process are known. We proposed the C-terminal region of SARAF as a potential negative regulator of the SOCE response in the context of TNBC. Unpublished data from our laboratory suggest that a mutant version of the SARAF protein (*i.e.,* $SARAF^{K326R}$) presents an increased interaction with STIM1 compared to the wild-type version. In addition, we have observed that the overexpression of $SARAF^{K326R}$ presents a greater reduction of the SOCE response in HEK293 cell model in comparison to wild wild-type version. Therefore, we expected that there would be a greater reduction of the SOCE response using mScarlet-C-$SARAF^{K326R}$ compared to the mScarlet-C-SARAF to the control condition.

We observed that the C-terminal region of SARAF is sufficient to reduce the SOCE response (Figures 3-7), having the same effect observed by Palty *et al*. (2012)[71]. However, we did not observe differences between the wild and mutant versions. This difference between the effect of the mutant version of SARAF when the protein is completely overexpressed versus when only the C-terminal is overexpressed could be because the ubiquitination of lysine 326 has a greater effect when the luminal region of SARAF is present. This suggests that the ubiquitination of SARAF in lysine 326 could have an allosteric effect on the N-terminal domain, enhancing its effect as a negative regulator of calcium entry, which is not observed when only the C-terminal region is present. The ubiquitination/non-ubiquitination of lysine 326 could affect the oligomeric state of the ER-luminal domain of SARAF[133,], acting as an allosteric modulation and affecting the normal stoichiometry of SARAF-STIM1 complex. Interestingly, it has been described that both the activation and biophysical properties of CRAC channels depend

on the stoichiometry between the different molecular entities involved in the formation of the CRAC channel such as STIM1/2, Orai1/2/3, SARAF, among others[66,133–136].

On the other hand, different studies have observed that the reduction of the SOCE response using pharmacological inhibitors or modification in the expression of positive or negative regulators of the SOCE response induces cell cycle arrest, less migration and/or invasion of neoplastic cells [127,129,137,138]. Particularly, with the use of the mScarlet-C-SARAF fragments, we did not observe changes in cell viability (Figure 10A-B), but we did observe a decrease in cell migration (Figures 11 and 12) and cell invasion (Figures 13 and 14) in MDA-MB-231 and 4T1 cells line *in vitro* and *in vivo* (Figure 21). Therefore, the C-terminal fragment of SARAF could reduce the metastasis of TNBC.

Interestingly, in contrast to the similar effects of the mScarlet-C-SARAF and mScarlet-C-SARAF^{K326R} fragments on the calcium entry between fragments, we found that the mutated version of mScarlet-C-SARAF^{K326R} had a greater effect on cell migration and invasion compared to the non-mutated mScarlet-C-SARAF. This indicates that the mutant version may be regulating other downstream signaling mechanisms that could be related to the strength of the SOCE response. There are different molecular mechanisms that could explain this effect:

The data on the dynamics of STIM1 cluster formation after the overexpression of the C-SARAF fragments indicate that the mutant version, although it does not affect the number of basal clusters and after TG stimulation, does present a slower formation rate in comparison to the control and the wild type version (Figure 5). Previous reports have suggested that STIM1 is required for calcium oscillations[139–141]. However, a recent study shows that STIM1 and STIM2 coordinate Ca^{2+} oscillation frequencies in response to different concentrations of agonists through IP3R activity[142]. Therefore, changes in the dynamics of STIM1 formation induced by the mutant version of the C-SARAF fragment could affect the timing of complex formation between the STIM-Orai-IP3R proteins and may affect the frequency or amplitude of calcium oscillations, allowing activate different targets such as NFAT1 and NFAT4 that have downstream targets.

In addition, STIM2 induces activated conformation of STIM1 to control Orai1 function, modulating function tunes the physiological response of cells[143.] Therefore, C-SARAF^{K326R} could also be involved in the association dynamics between STIM1/STIM2. This could explain the fact that although there are no differences in the net calcium signaling between the mScarlet-C-SARAF fragments, there are differences in migration and invasion (Figures 11-14, 21).

Another possible explanation is that the mScarlet-C-SARAF^{K326R} could differentially regulate mechanisms associated with calcium entry independent of internal reservoirs, also called SICE. Recent studies have reported the role of SICE in regulating breast cancer processes [144,145]. The store-independent, arachidonic acid-activated ARC channels, like CRAC channels, are highly Ca^{2+}-selective and low conductance channels. The molecular architecture is a pentameric assembly of Orai and Orai3 subunits and is regulated by STIM1[146,147]. Interestingly, Albarrán *et al.* (2016) described SARAF's participation in the regulation of this channel[136]. Furthermore, Chamlali *et al*. (2021) recently described that the Orai3 channel regulates FAK activity related to focal adhesion assembly and dynamic of the cytoskeleton in MDA-MB-231 cells through calcium-dependent and independent mechanisms[148]. Therefore, the C-SARAF mutant could affect the activity of the ARC or Orai3 channels, affecting the migration of these cells through focal adhesion and cytoskeleton dynamics (Figures 17 and 18). In this same sense, other molecular entities that C-SARAF^{K326R} could be differentially regulated compared to the wild-type version involved in SICE, are SPCA2-Orai11-Kv10.1[149–151] protein complex.

In addition, there is another mechanism that in recent years has become relevant in breast cancer and the co-regulation described between the Orai1 channel and the Ca^{2+} activated K^+ ion channel SK3[152–154]. Tiffner *et al.* (2021) recently identified that cytosolic strands and Orai1 channel pore residues are critical for functional communication with SK3. Furthermore, STIM1 has a bimodal role in the regulation of SK3-Orai1, where under physiological conditions, STIM1 interferes with the SK3-Orai1 interaction by significantly decreasing the co-localization of channels during activity. STIM1-Orai1 and the associated Ca^{2+} entry promote the co-localization of the Orai1-SK3 channel and the activation of K^+ currents[155]. In this sense, since STIM is key for

Orai1-SK3 dynamic regulation, SARAF could be involved, specifically the mutant version of the C-terminal region, altering the malignancy characteristics of neoplastic cells.[152–154]

Moreover, others such as EFHB[86], TMEM97[156], AC8[157], and PGRMC1[88] are upregulated, and that contributes to the increase in the SOCE response in the breast cancer context. Therefore, they become potential therapeutic targets. Considering that the formation of the STIM-Orai complex and all these possible interactions during the SOCE response, mScarlet-C-SARAF^{K326R} could be differentially regulating this complex composition and/or dynamics of the SARAF-STIM1-ORAI1 proteins interaction along with the interaction of other proteins (EFHB[86], TMEM97[156], AC8[157], and PGRMC1[88]). mScarlet-C-SARAF^{K326R} could also be regulating the interaction or participation of other channels such as TRPC6[127,129] and TRPC1[158,159], or Mitochondrial Ca^{2+} uniporter[137] restricting cell migration, as reported by different groups in MDA-MB-231 cells. Therefore, mScarlet-C-SARAF^{K326R} by reworking the potential interactors present in the STIM-ORAI complex could be modifying the calcium microdomains, altering the size, number of the STIM-Orai cluster, and activation level of the channel, which the sum generates the same calcium influx for both mScarlet-C-SARAF versions but at the molecular level it generates the differential activation of transcription factors or calcium-dependent proteins that are located near the CRAC channel. This was evidenced by Lin *et al*. in (2019), who particularly observed that NFAT and c-fos have different requirements in terms of the number of clusters and the flow of calcium that pass through them due to their activation [160].

According to the role of SARAF in the SOCE response, this could be dependent on the tissue, physiological, and pathophysiological context. Particularly in breast cancer, Jardin *et al.* (2021) observed that the expression of SARAF has different effects on the SOCE response and cell migration in non-tumor, Luminal A, and Triple negative human cell lines. In MDA-MB-231 cells, the silencing of SARAF induces an increase in the SOCE response[138] as expected. However, contrary to the project they observed that the silencing of SARAF induces a decrease in collective cell migration [138]. This difference could be due to regulatory mechanisms of SARAF activity that the N-terminal region could exert in different cellular contexts and that by using only the C-terminal

region of the protein these mechanisms would be absent. Moreover, SARAF has recently been described as having a dual role in the SOCE response, where after reticular calcium depletion SARAF promotes the active conformation of STIM1 promoting the initial activation of the SOCE response and after its subsequent dissociation[72]. Possibly the soluble mScarlet-C-SARAF fragment prevents its interaction with the endogenous SARAF protein and therefore restricts the dual regulation that this protein presents where the N-terminal region could be involved, which is absent in the mScarlet-C-SARAF fragment.

Lastly, given that KCTD5 increases its expression in breast cancer and promotes cell migration through the activity of TRPM4 [91] mScarlet-C-SARAF^{K326R} could be acting as a competitive inhibitor preventing the interaction of KCTD5, an adapter of Ubiquitin E3 ligase with other substrates [161] involved in the cell migration and invasion process such as TRPM4 [91], this could explain the fact that although there are no differences in the magnitude of the SOCE response evoked when mScarlet-C-SARAF and mScarlet-C-SARAF^{K326R} are overexpressed if differences are observed in the migration and invasion of tumor cells, with mScarlet-C-SARAF^{K326R} having a more powerful effect compared to the wild-type version. Currently, Cullin-RING ligases (CRLs), the largest family of E3 ubiquitin ligases, have become an attractive target for drug discovery, primarily due the abnormal expressions of CRLs and their substrate proteins are associated with human diseases[162], so the development of small molecules that target CRLs has been enhanced. The potential inhibition points for disrupting the interaction between the components of CRL complex can be classified into six groups: (1) group 1, targeting the transfer of ubiquitin from the E2-Ub conjugate to the lysine residues on the substrate; (2) group 2, disrupting the interaction between Cullin and RING protein; (3) group 3, inhibiting the neddylation of Cullins; (4) group 4, disrupting the interaction between Cullin and adaptor; (5) group 5, targeting the interaction between adaptor and receptor; (6) group 6, targeting the interaction between receptor and substrate [163], being able to belong mScarlet-C-SARAF^{K326R} to this last group.

Moreover, under the observed effects on cell migration and invasion in TNBC cells after the overexpression of mScarlet-C-SARAF fragments, we observed a decrease in the density of focal adhesions and disassembly rate and changes in the

organization of actin during the cell spreading adhesion process (Figures 15-18). These data are consistent with other publications that associate the reduction of the SOCE response with a reduction in migration and invasion of neoplastic cells [39,137,138,157,164–166]. In this context, Chakraborty *et al*. (2016) described the use of phemindole, a synthetic dietary indol that presents antitumor characteristics and is proposed as a potential compound for pharmacological use for chemotherapy that favors the reduction of STIM1 expression by inducing less interaction between STIM1-Orai, this generates a decrease in cell migration *in vitro* through the regulation of FAK, also observe a reduction in tumor growth in an *in vivo* model[165]. Therefore, the same pathways could be affecting the mScarlet-C-SARAF fragments. Considering that these would generate a reduction in the interaction between STIM-Orai. Another mechanism is that mScarlet-C-SARAF could be interfering in the interaction between PAK1 and STIM. Jeon *et al*. (2018) described that PAK1, a p21-activated kinase, which is a downstream effector of GTPases, modulates SOCE-dependent calcium mobilization and localizes with STIM1. Both proteins basally colocalize in the cytosol however when using a nascent adhesion inducer, such as phorbol 12,13-dibutyrate (PDBu) both proteins colocalize to peripheral vinculin-positive adhesions[167]. In addition, it has recently been described that PAK1 interacts with and phosphorylates calcium/calmodulin-dependent protein kinase II (CaMKII) in the context of breast cancer[168]. Interestingly, another protein has been described to regulate the conformational change of STIM1, promoting its activation in the context of TNBC. Lee *et al*. (2022) determined that PGRMC1, a protein that increases its expression in TNBC, promotes the SOCE response in addition to regulating the turnover of focal adhesions and the formation of actomyosin[88]. Thus, the mScarlet-C-SARAF fragments could interact directly with STIM1, regulating its conformational change, and having an impact on the reduction in cell migration and invasion. In the case of the mutant version, this modulation could be less dynamic compared to the wild-type version.

In the context of cell invasion, STIM-Orai1 are essential in orchestrating the activation of metalloproteinases[169] and the formation of podosomes[40,170] that allow the degradation and migration of neoplastic cells through the extracellular matrix. Sun *et al*. (2014), described Orai oscillation as an impact on invadosome formation and

activation of metalloproteinase MT1-MPP[169]. In addition, Rizaner *et al*. (2016), related the highly metastatic potential of MDA-MB-231 cells, which presented spontaneous Ca^{2+} oscillations, while such oscillations were not observed in MCF-7 cells, which present less metastatic potential [171]. Given that it has been reported that in MDA-MB-231 cells the expression of Orai1 predominates compared to Orai2 and that this increase in the Orai1/Orai2 ratio is associated with the activation of NFAT1 with low concentrations of agonists[124]. Taken together, these data would indicate that mScarlet-C-SARAF could be mainly regulating Orai1, which would influence the activation of MPP. Furthermore, different studies have indicated the relevance of STIM1-Orai1 activity in the formation of podosomes[40,169], relevant structures in the invasion process. Although the molecular mechanism involved is not completely known, studies suggest that the activity of STIM1-Orai1 would regulate podosomes rosettes dynamics through the effect on the regulation of actomyosin reorganization[172], so the C-terminal SARAF fragments by reducing SOCE could affect in the formation of these structures and therefore reduce the invasion of cells.

The effect of mScarlet-C-SARAF overexpression in a murine model of breast cancer as a lower percentage of portal veins affected by infiltrating tumor cells are supported by the decrease in cell migration and invasion observed *in vitro* assays when we overexpress the mScarlet-C-SARAF fragments. On the other hand, in the last decade, tumor-infiltrating lymphocytes (TILs) have been established as a biological biomarker that improves discrimination over prognostic clinical and pathologic staging for early-stage TNBC.[173]. Where the presence of TILs in the tumor microenvironment can predict responses not only to neoadjuvant but also to adjuvant chemotherapy treatments. Thus, a high number of TILs correlates with increased pathologic complete responses in TNBC. We observed that mScarlet-C-SARAF^{K326R} overexpressed in the primary tumor presented a high number of TILs in comparison with control. This effect may be associated with the fact that the mScarlet-C-SARAF fragments promote a senescent secretory phenotype, where tumor cells generate a proinflammatory microenvironment by attracting lymphocytes after the production of proinflammatory cytokines[174]. Indeed, in the prostate cancer context, STIM1 has been observed to promote cell senescence[175]. At the molecular level, C-SARAF fragments by reducing

the activation of NFAT1, could promote the expression of IRF8[109]. Although its specific function in breast cancer tumor cells is unknown, its increase has been associated with promoting the recruitment of CD8 lymphocytes[176] which are associated with a good prognostic.[11,102] Moreover, high TILs could be associated with a better response to pharmacological treatments and therefore a better prognosis when mScarlet-C-SARAF and mScarlet-C-SARAF^{K326R} are overexpressed in tumor cells.

Currently, the lack of drugs remains a problem despite attempts to use several compounds as selective pharmacological modulators of Orai1-STIM1 in different models[112]. Therefore, the design and development of drugs targeting the mechanisms that regulate Orai1-STIM1 activity could lead to complementary therapeutic strategies for diseases such as cancer. The most direct way of regulating the activity of a therapeutic target is protein-protein interaction modulation, since it allows affecting only the cellular pathway associated with the interaction, obtaining minimal off-target effects [113–115]. The mechanisms associated with the regulation of protein-protein interactions are that modulators can stabilize or inhibit the interaction through their direct binding to the protein-protein interface or through the binding of allosteric sites. There are 3 types of modulators: small molecules, antibodies, and peptides[116]. Using peptides, specifically Cell-Penetrating Peptides (CPPs), for disease-related Protein-Protein Interaction (PPI) has been successful in therapeutic approaches, including modulation of ion channel-related PPI.[99,113–115,117.] CPPs have shown potential for the delivery of a wide range of molecules, including large active proteins to enter cells via endocytosis. Normally is a basic peptide composed of 5-30 amino acids[118]. One type of carrier is a peptide sequence derived from the transcription transactivator of the human immunodeficiency virus (HIV) (called TAT) that penetrates the cells with low cytotoxic effects in a receptor-independent and concentration-dependent manner[119]. Moreover, TAT-CPP-based peptides have been used as an efficient noninvasive delivery system in several tissues and tumors [119,120] including breast cancer model[121–123]. As such, CPPs designed to modulate specific PPIs might constitute a powerful strategy for drug development against different diseases.

Based on the observed effect of the C-terminal fragments of SARAF on the SOCE response, migration, and invasion in neoplastic cells, we tested the use of

penetrating TAT peptides that contain a smaller portion of the C-terminal region of SARAF corresponding to amino acid 310 to 339 (Figure 23D).

The TAT peptides were incubated for 24 hours in MDA-MB-231 cells, subsequently, we evaluated their effect on the SOCE response by applying the same protocol used in previous experiments. Interestingly, we observed that both wild-type and mutant TAT-C-SARAF peptides equally reduce the SOCE response compared to the control (Figure 23 A-C). This suggests that amino acids 310 to 339 (TAT-C-SARAF) are sufficient to obtain the same effect observed with fragments 195 to 339 (mScarlet-C-SARAF).

After the calcium recordings were made with the cells treated with the TAT-C-SARAF peptides, cells were fixed as described in materials and methods to evaluate the penetrance of the peptide and its effect on focal adhesions by immunofluorescence (Figure 24). We showed that the peptides penetrated the registered cells and, interestingly, we observed that the TAT-C-SARAF peptides increased the size (Figure 24 B) and reduced the number of focal adhesions (Figure 24 C), a phenotype associated with fewer migratory cells[87].

Therefore, the use of these TAT peptides could have potential pharmacological use, however, more studies on their role in the molecular mechanism in the regulation of SOCE and in the processes of cell migration and invasion are required.

CONCLUSION

mScarlet-C-SARAF fragments reduce calcium influx dependent on the SOCE response in human and murine TNBC cell lines, in addition to reducing their migratory and invasive phenotype. The data also suggest that it allows for enhancing the immune response itself, sensitizing the primary tumor to the effect of conventional therapies, possibly increasing its rate of treatment success.

ANNEXES

FUTURE PROJECTIONS

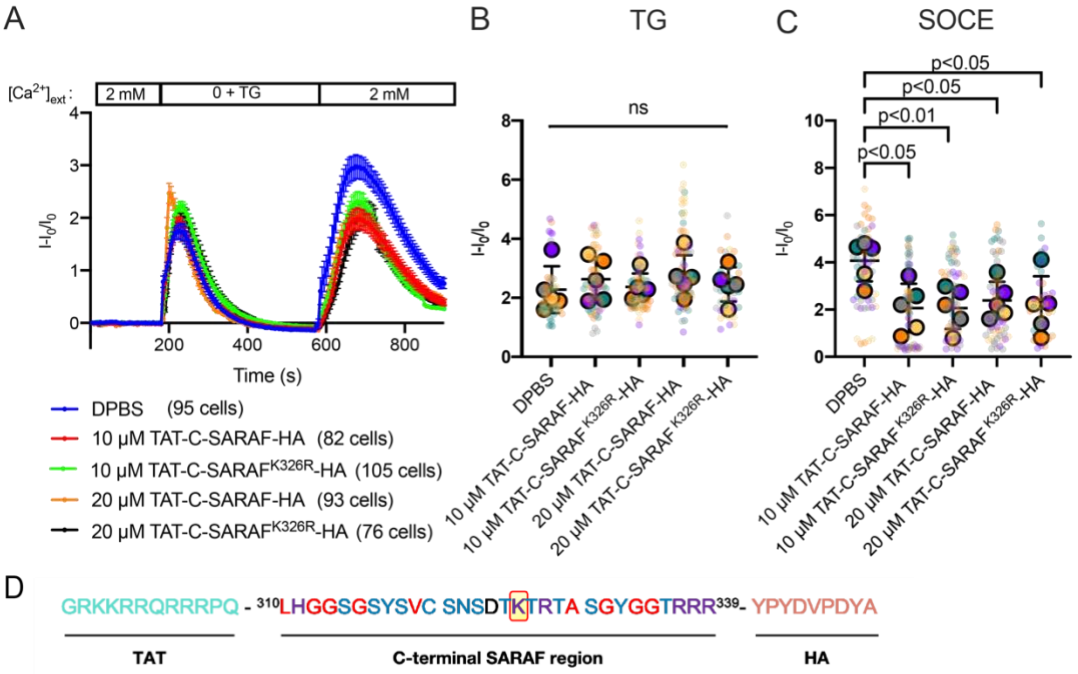

Figure 23. TAT-C-SARAF peptides decrease the SOCE response in the human TNBC cell line.

A Representative graph of SOCE response. TAT-C-SARAF and TAT-C-SARAF^{K326R} were incubated in MDA-MB-231 cells which were loaded with Fura-2 AM and then calcium imaging was performed. The protocol used consisted of 3 minutes with Ringer's solution of 2 mM $CaCl_2$, then Ca^{2+} depletion was induced with calcium-free Ringer's solution with 1 mM EGTA and 2 μM of thapsigargin (TG) for 7 minutes. Finally, the solution is changed to Ringer's 2 mM $CaCl_2$ to induce calcium entry. **B-C** Representative graph of maximum peak TG-induced and maximum Ca^{2+} influx in MDA-MB-231 SOCE response respectively. Each independent experiment is represented with color and expressed as individual data per cell and as average per experiment (n=5). Statistical analysis used in graphs B and C was One-way ANOVA Dunn's multiple comparisons test. **D** Amino acid sequence corresponding to TAT peptide incubated in MDA-MB-231 cells.

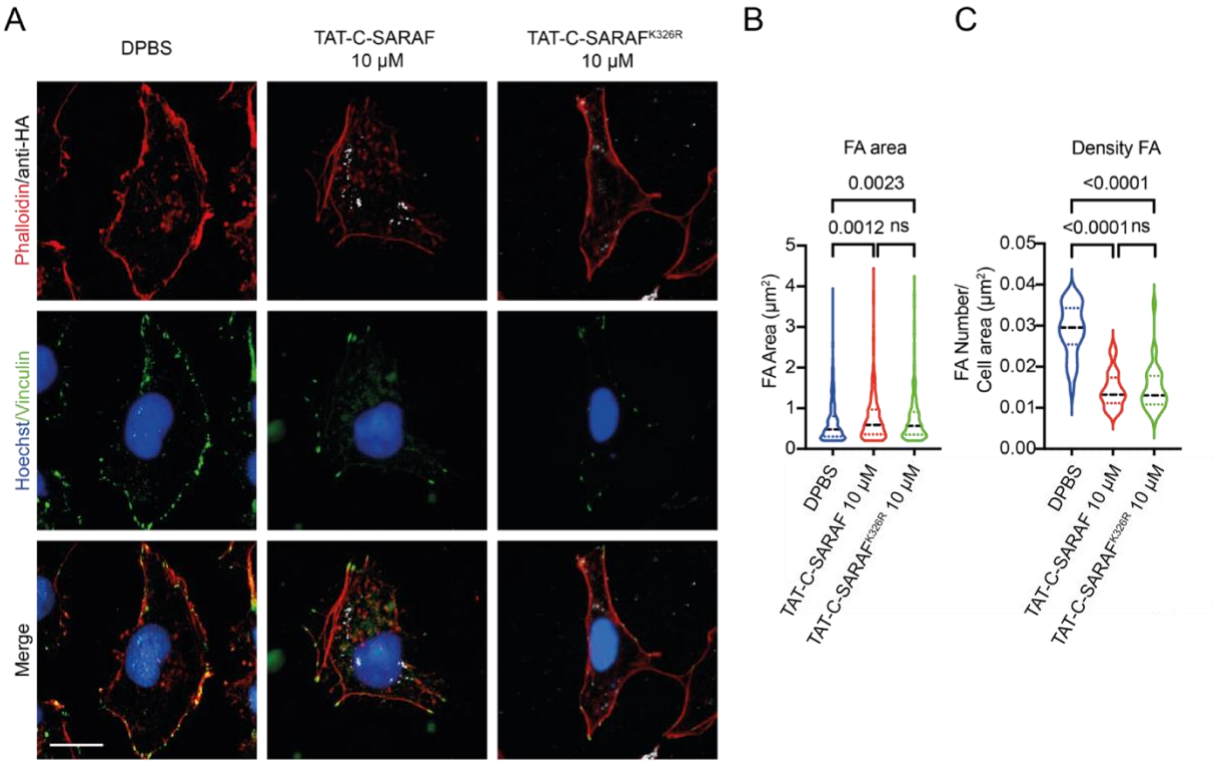

Figure 24. TAT-C-SARAF peptides decrease the number and size of focal adhesion in the human TNBC cell line.

A Representative immunofluorescence panel of MDA-MB-231 cells treated with 10 µM of TAT peptides during 24 h. Red corresponds to actin filaments (phalloidin), green corresponds to focal adhesion (vinculin), blue corresponds to the nucleus (Hoechst) and white corresponds to TAT-C-SARAF peptide tagged with HA (anti-HA). **B** Graph of the area of focal adhesion. **C** Graph of the density of focal adhesion. Five independent experiments were analyzed. Scale bar= 5 µm. The statistical analysis used was the One-way ANOVA Dunn's test.

ANIMAL PROTOCOL

VID INVESTIGACIÓN INNOVACIÓN CREACIÓN ARTÍSTICA
Vicerrectoría de Investigación y Desarrollo
UNIVERSIDAD DE CHILE

CICUA
COMITÉ INSTITUCIONAL DE CUIDADO Y USO DE ANIMALES

Santiago, 23 de junio de 2020

Certificado Nº: **20382-MED-UCH**

CERTIFICADO

El Comité Institucional de Cuidado y Uso de Animales (CICUA) de la Universidad de Chile, certifica que en el Protocolo **CBA 1130 FMUCH,** del Proyecto de Investigación titulado: **"Regulación de la actividad de los canales Orai1-STIM1 por la ubiquitinación de SARAF dependiente de KCTD5 y su rol durante la migración celular",** de la Investigadora **María Paz Saldías Maulén**, Tesista del Programa de Doctorado Ciencias Biomédicas, Facultad de Medicina, Universidad de Chile, y cuyo Académico Patrocinante y Responsable es el **Dr. Oscar Alejandro Cerda Arancibia**, Profesor Asociado, Programa de Biología Celular y Molecular, ICBM, Facultad de Medicina, Universidad de Chile, no se plantean acciones en sus procedimientos que contravengan las normas de Bioética de manejo y cuidado de animales. Así mismo, la metodología experimental planteada satisface lo estipulado en el Programa Institucional de Cuidado y Uso de Animales de la Universidad de Chile.

Los Investigadores se han comprometido a la ejecución de este proyecto dentro de las especificaciones señaladas en el protocolo revisado y autorizado por el CICUA, a mantener los procedimientos experimentales planteados y a no realizar ninguna modificación sin previa aprobación por parte de este Comité.

Se otorga la presente certificación para el uso de un total de **189** ratones de la especie *Mus musculus* SPF Cepa Balb/c, obtenidos del Bioterio Central de la Facultad de Medicina, Universidad de Chile, desde **abril de 2021 hasta marzo de 2024**, tiempo estimado de ejecución del estudio, el cual será financiado por **Proyecto Fondecyt Regular Nro. 1200917.**

*El CICUA de la Universidad de Chile, forma parte de la Vicerrectoría de Investigación y Desarrollo, y está constituido por 53 miembros: 5 médicos veterinarios, 39 académicos (12 de ellos médicos veterinarios), y 9 miembros no asociados a la academia o investigación, y que cuentan con experiencia en bioética relacionada a mantención y uso de animales. El certificado que emite el Comité procede de la aprobación del "**Protocolo de Manejo y Cuidado de Animales**" después de un estudio acucioso y de la acogida de los investigadores de las observaciones exigidas por el Comité.*

Comité Institucional de Cuidado y Uso de los Animales ★ CICUA VID ★ Universidad de Chile

Ronald Vargas Casanova
Director
CICUA – VID
Universidad de Chile

Dr. Emilio Herrera Videla
Presidente
CICUA - VID
Universidad de Chile

PUBLICATIONS

1. **Saldías MP**, Cruz P, Silva I, Orellana-Serradell O, Lavanderos B, Maureira D, Pinto R, Cerda O. The cytoplasmic region of SARAF reduces triple-negative breast cancer metastasis through the regulation of the Store Operated Calcium Entry. Int J Mol Sci. (2023), DOI: 10.3390/ijms24065306.
2. **Saldías MP**, Maureira D, Orellana-Serradell O, Silva I, Lavanderos B, Cruz P, Torres C, Cáceres M, Cerda O. TRP channels interactome as a novel therapeutic target in breast cancer. Frontiers in Oncology (2021), DOI: 10.3389/fonc.2021.621614.
3. Garrido M, Morales D, **Saldías MP,** Fernández C, Villalobos V, Cerda O, Cáceres M. Cellular response of human apical papilla cells to calcium hydroxide and tricalcium silicate-based cements. BMC Oral Health (2021), DOI: 10.1186/s12903-021-01467-6
4. Lavanderos B, Silva I, Cruz P, Orellana-Serradell O, **Saldías MP**, Cerda O. TRP Channels Regulation of Rho GTPases in Brain Context and Diseases. Front Cell Dev Biol. (2020), DOI: 10.3389/fcell.2020.582975
5. Rivas J, Díaz N, Silva I, Morales D, Lavanderos B, Álvarez A, **Saldías MP**, Pulgar E, Cruz P, Maureira D, Flores G, Colombo A, Blanco C, Contreras HR, Jaña F, Gallegos I, Concha ML, Vergara-Jaque A, Poblete H, González W, Varela D, Trimmer JS, Cáceres M, Cerda O. KCTD5, a novel TRPM4-regulatory protein required for cell migration as a new predictor for breast cancer prognosis. FASEB J. (2020), DOI: 10.1096/fj.201901195RRR

REFERENCES

1. Ferlay, J. *et al.* Estimating the global cancer incidence and mortality in 2018: GLOBOCAN sources and methods. *Int J Cancer* **144**, 1941–1953 (2019).
2. Bray, F. *et al.* Global cancer statistics 2018: GLOBOCAN estimates of incidence and mortality worldwide for 36 cancers in 185 countries. *CA Cancer J Clin* **68**, 394–424 (2018).
3. Harbeck, N. *et al.* Breast cancer. *Nat Rev Dis Primers* **5**, 66 (2019).
4. Bianchini, G., Balko, J. M., Mayer, I. A., Sanders, M. E. & Gianni, L. Triple-negative breast cancer: challenges and opportunities of a heterogeneous disease. *Nat Rev Clin Oncol* **13**, 674–690 (2016).
5. Badve, S. *et al.* Basal-like and triple-negative breast cancers: a critical review with an emphasis on the implications for pathologists and oncologists. *Mod Pathol* **24**, 157–167 (2011).
6. Marra, A., Trapani, D., Viale, G., Criscitiello, C. & Curigliano, G. Practical classification of triple-negative breast cancer: intratumoral heterogeneity, mechanisms of drug resistance, and novel therapies. *NPJ Breast Cancer* **6**, 54 (2020).
7. Livasy, C. A. *et al.* Phenotypic evaluation of the basal-like subtype of invasive breast carcinoma. *Modern Pathology* **19**, 264–271 (2006).
8. Thike, A. A. *et al.* Triple-negative breast cancer: clinicopathological characteristics and relationship with basal-like breast cancer. *Modern Pathology* **23**, 123–133 (2010).
9. Weisman, P. S. *et al.* Genetic alterations of triple negative breast cancer by targeted next-generation sequencing and correlation with tumor morphology. *Modern Pathology 2016 29:5* **29**, 476–488 (2016).
10. Li, J. J., Tsang, J. Y. & Tse, G. M. Tumor Microenvironment in Breast Cancer—Updates on Therapeutic Implications and Pathologic Assessment. *Cancers (Basel)* **13**, 4233 (2021).
11. Hendry, S. *et al.* Assessing Tumor-infiltrating Lymphocytes in Solid Tumors: A Practical Review for Pathologists and Proposal for a Standardized Method From the International Immunooncology Biomarkers Working Group: Part 1: Assessing the Host Immune Response, TILs in Invasive Breast Carcinoma and Ductal Carcinoma In Situ, Metastatic Tumor Deposits and Areas for Further Research. *Adv Anat Pathol* **24**, 235–251 (2017).
12. de Melo Gagliato, D. *et al.* Tumor-infiltrating lymphocytes in Breast Cancer and implications for clinical practice. *Biochim Biophys Acta Rev Cancer* **1868**, 527–537 (2017).
13. Baxevanis, C. N., Fortis, S. P. & Perez, S. A. The balance between breast cancer and the immune system: Challenges for prognosis and clinical benefit from immunotherapies. *Semin Cancer Biol* **72**, 76–89 (2021).
14. Gómez-Aleza, C. *et al.* Inhibition of RANK signaling in breast cancer induces an anti-tumor immune response orchestrated by CD8+ T cells. *Nat Commun* **11**, (2020).
15. Dushyanthen, S. *et al.* Agonist immunotherapy restores T cell function following MEK inhibition improving efficacy in breast cancer. *Nat Commun* **8**, (2017).

16. Neophytou, C. M., Panagi, M., Stylianopoulos, T. & Papageorgis, P. The Role of Tumor Microenvironment in Cancer Metastasis: Molecular Mechanisms and Therapeutic Opportunities. *Cancers (Basel)* **13**, (2021).
17. Lambert, A. W., Pattabiraman, D. R. & Weinberg, R. A. Emerging Biological Principles of Metastasis. *Cell* **168**, 670–691 (2017).
18. Chaffer, C. L. & Weinberg, R. A. A perspective on cancer cell metastasis. *Science (1979)* **331**, 1559–1564 (2011).
19. van Zijl, F., Krupitza, G. & Mikulits, W. Initial steps of metastasis: Cell invasion and endothelial transmigration. *Mutation Research/Reviews in Mutation Research* **728**, 23–34 (2011).
20. Stewart, T. A., Yapa, K. T. & Monteith, G. R. Altered calcium signaling in cancer cells. *Biochim Biophys Acta* **1848**, 2502–2511 (2015).
21. Ridley, A. J. *et al.* Cell migration: integrating signals from front to back. *Science (1979)* **302**, 1704–1709 (2003).
22. Cáceres, M. *et al.* TRPM4 Is a Novel Component of the Adhesome Required for Focal Adhesion Disassembly, Migration and Contractility. *PLoS One* **10**, e0130540 (2015).
23. Stuelten, C. H., Parent, C. A. & Montell, D. J. Cell motility in cancer invasion and metastasis: insights from simple model organisms. *Nat Rev Cancer* **18**, 296–312 (2018).
24. Aseervatham, J. Cytoskeletal Remodeling in Cancer. *Biology (Basel)* **9**, 1–40 (2020).
25. Parsons, J. T., Horwitz, A. R. & Schwartz, M. A. Cell adhesion: integrating cytoskeletal dynamics and cellular tension. *Nat Rev Mol Cell Biol* **11**, 633–643 (2010).
26. Li, X. & Wang, J. Mechanical tumor microenvironment and transduction: cytoskeleton mediates cancer cell invasion and metastasis. *Int J Biol Sci* **16**, 2014 (2020).
27. Howe, A. K. Cross-talk between calcium and protein kinase A in the regulation of cell migration. *Curr Opin Cell Biol* **23**, 554–561 (2011).
28. Kappel, S., Borgström, A., Stokłosa, P., Dörr, K. & Peinelt, C. Store-operated calcium entry in disease: Beyond STIM/Orai expression levels. *Semin Cell Dev Biol* **94**, 66–73 (2019).
29. Hooper, R. *et al.* Novel Protein Kinase C-Mediated Control of Orai1 Function in Invasive Melanoma. *Mol Cell Biol* **35**, 2790–2798 (2015).
30. Stanisz, H. *et al.* Inverse regulation of melanoma growth and migration by Orai1/STIM2-dependent calcium entry. *Pigment Cell Melanoma Res* **27**, 442–453 (2014).
31. Sun, J. *et al.* STIM1- and Orai1-mediated Ca2+ oscillation orchestrates invadopodium formation and melanoma invasion. *Journal of Cell Biology* **207**, 535–548 (2014).
32. Motiani, R. K. *et al.* STIM1 and Orai1 mediate CRAC channel activity and are essential for human glioblastoma invasion. *Pflugers Arch* **465**, 1249–1260 (2013).
33. Kim, J. H. *et al.* Orai1 and STIM1 are critical for cell migration and proliferation of clear cell renal cell carcinoma. *Biochem Biophys Res Commun* **448**, 76–82 (2014).

34. Yang, N. *et al.* Blockade of store-operated Ca(2+) entry inhibits hepatocarcinoma cell migration and invasion by regulating focal adhesion turnover. *Cancer Lett* **330**, 163–169 (2013).
35. Boutin, B. *et al.* Endoplasmic reticulum Ca(2+) content decrease by PKA-dependent hyperphosphorylation of type 1 IP3 receptor contributes to prostate cancer cell resistance to androgen deprivation. *Cell Calcium* **57**, 312–320 (2015).
36. Chen, Y. F. *et al.* Calcium store sensor stromal-interaction molecule 1-dependent signaling plays an important role in cervical cancer growth, migration, and angiogenesis. *Proc Natl Acad Sci U S A* **108**, 15225–15230 (2011).
37. Jardin, I., Lopez, J. J., Salido, G. M. & Rosado, J. A. Store-Operated Ca 2+ Entry in Breast Cancer Cells: Remodeling and Functional Role. *Int J Mol Sci* **19**, (2018).
38. Motiani, R. K., Abdullaev, I. F. & Trebak, M. A novel native store-operated calcium channel encoded by Orai3: Selective requirement of Orai3 versus Orai1 in estrogen receptor-positive versus estrogen receptor-negative breast cancer cells. *Journal of Biological Chemistry* **285**, 19173–19183 (2010).
39. McAndrew, D. *et al.* ORAI1-mediated calcium influx in lactation and in breast cancer. *Mol Cancer Ther* **10**, 448–460 (2011).
40. Chen, Y. W., Chen, Y. F., Chiu, W. T., Chen, H. C. & Shen, M. R. STIM1-dependent Ca2+ signaling regulates podosome formation to facilitate cancer cell invasion. *Sci Rep* **7**, 11523 (2017).
41. Parekh, A. B. & Putney, J. W. Store-operated calcium channels. *Physiol Rev* **85**, 757–810 (2005).
42. Liou, J. *et al.* STIM is a Ca2+ sensor essential for Ca2+-store-depletion-triggered Ca2+ influx. *Curr Biol* **15**, 1235–1241 (2005).
43. Roos, J. *et al.* STIM1, an essential and conserved component of store-operated Ca 2+ channel function. *Journal of Cell Biology* **169**, 435–445 (2005).
44. Feske, S. *et al.* A mutation in Orai1 causes immune deficiency by abrogating CRAC channel function. *Nature* **441**, 179–185 (2006).
45. Vig, M. *et al.* CRACM1 is a plasma membrane protein essential for store-operated Ca2+ entry. *Science (1979)* **312**, 1220–1223 (2006).
46. Zhang, S. L. *et al.* Genome-wide RNAi screen of Ca(2+) influx identifies genes that regulate Ca(2+) release-activated Ca(2+) channel activity. *Proc Natl Acad Sci U S A* **103**, 9357–9362 (2006).
47. Park, C. Y. *et al.* STIM1 Clusters and Activates CRAC Channels via Direct Binding of a Cytosolic Domain to Orai1. *Cell* **136**, 876–890 (2009).
48. Muik, M. *et al.* A Cytosolic Homomerization and a Modulatory Domain within STIM1 C Terminus Determine Coupling to ORAI1 Channels. *J Biol Chem* **284**, 8421–8426 (2009).
49. Rathner, P. *et al.* Interhelical interactions within the STIM1 CC1 domain modulate CRAC channel activation. *Nat Chem Biol* (2020) doi:10.1038/s41589-020-00672-8.
50. Muik, M. *et al.* Dynamic coupling of the putative coiled-coil domain of ORAI1 with STIM1 mediates ORAI1 channel activation. *Journal of Biological Chemistry* **283**, 8014–8022 (2008).
51. Zhou, Y. *et al.* Initial activation of STIM1, the regulator of store-operated calcium entry. *Nat Struct Mol Biol* **20**, 973–981 (2013).

52. Korzeniowski, M. K., Manjarres, I. M., Varnai, P. & Balla, T. Activation of STIM1-Orai1 Involves an Intramolecular Switching Mechanism. *Sci Signal* **3**, ra82–ra82 (2010).
53. Stathopulos, P. B. *et al.* STIM1/Orai1 coiled-coil interplay in the regulation of store-operated calcium entry. *Nat Commun* **4**, 2963 (2013).
54. Zhou, Y. *et al.* The STIM-Orai coupling interface and gating of the Orai1 channel. *Cell Calcium* (2017) doi:10.1016/j.ceca.2017.01.001.
55. Tiffner, A., Maltan, L., Weiß, S. & Derler, I. The Orai Pore Opening Mechanism. *Int J Mol Sci* **22**, 1–33 (2021).
56. Dong, H. *et al.* Toward a Model for Activation of Orai Channel. *iScience* **16**, 356–367 (2019).
57. Zhou, Y. *et al.* The remote allosteric control of Orai channel gating. *PLoS Biol* **17**, 1–9 (2019).
58. Yuan, J. P. *et al.* SOAR and the polybasic STIM1 domains gate and regulate Orai channels. *Nat Cell Biol* **11**, 337–343 (2009).
59. Hoth, M. CRAC channels, calcium, and cancer in light of the driver and passenger concept. *Biochim Biophys Acta* **1863**, 1408–1417 (2016).
60. Derler, I., Jardin, I. & Romanin, C. Molecular mechanisms of STIM/Orai communication. *Am J Physiol Cell Physiol* (2016) doi:10.1152/ajpcell.00007.2016.
61. Mullins, F. M., Park, C. Y., Dolmetsch, R. E. & Lewis, R. S. STIM1 and calmodulin interact with Orai1 to induce Ca2+-dependent inactivation of CRAC channels. *Proc Natl Acad Sci U S A* **106**, 15495–15500 (2009).
62. Derler, I. *et al.* A Ca2(+)release-activated Ca2(+) (CRAC) modulatory domain (CMD) within STIM1 mediates fast Ca2(+)-dependent inactivation of ORAI1 channels. *J Biol Chem* **284**, 24933–24938 (2009).
63. Zweifach, A. & Lewis, R. S. Rapid inactivation of depletion-activated calcium current (ICRAC) due to local calcium feedback. *J Gen Physiol* **105**, 209–226 (1995).
64. Lee, K. P. *et al.* Molecular determinants of fast Ca2+-dependent inactivation and gating of the Orai channels. *Proc Natl Acad Sci U S A* **106**, 14687–14692 (2009).
65. Scrimgeour, N., Litjens, T., Ma, L., Barritt, G. J. & Rychkov, G. Y. Properties of Orai1 mediated store-operated current depend on the expression levels of STIM1 and Orai1 proteins. *J Physiol* **587**, 2903–2918 (2009).
66. Scrimgeour, N. R., Wilson, D. P., Barritt, G. J. & Rychkov, G. Y. Structural and stoichiometric determinants of Ca2+ release-activated Ca2+ (CRAC) channel Ca2+-dependent inactivation. *Biochim Biophys Acta* **1838**, 1281–1287 (2014).
67. Parekh, A. B. Slow feedback inhibition of calcium release-activated calcium current by calcium entry. *J Biol Chem* **273**, 14925–14932 (1998).
68. Zweifach, A. & Lewis, R. S. Slow calcium-dependent inactivation of depletion-activated calcium current. Store-dependent and -independent mechanisms. *J Biol Chem* **270**, 14445–14451 (1995).
69. Li, X. *et al.* Calmodulin dissociates the STIM1-Orai1 complex and STIM1 oligomers. *Nat Commun* **8**, (2017).
70. Jha, A. *et al.* The STIM1 CTID domain determines access of SARAF to SOAR to regulate Orai1 channel function. *J Cell Biol* **202**, 71–79 (2013).

71. Palty, R., Raveh, A., Kaminsky, I., Meller, R. & Reuveny, E. SARAF inactivates the store operated calcium entry machinery to prevent excess calcium refilling. *Cell* **149**, 425–438 (2012).
72. Zomot, E., Achildiev Cohen, H., Dagan, I., Militsin, R. & Palty, R. Bidirectional regulation of calcium release–activated calcium (CRAC) channel by SARAF. *Journal of Cell Biology* **220**, (2021).
73. Stathopulos, P. B., Zheng, L., Li, G. Y., Plevin, M. J. & Ikura, M. Structural and mechanistic insights into STIM1-mediated initiation of store-operated calcium entry. *Cell* **135**, 110–122 (2008).
74. Kawasaki, T., Lange, I. & Feske, S. A minimal regulatory domain in the C terminus of STIM1 binds to and activates ORAI1 CRAC channels. *Biochem Biophys Res Commun* **385**, 49–54 (2009).
75. Liou, J., Fivaz, M., Inoue, T. & Meyer, T. Live-cell imaging reveals sequential oligomerization and local plasma membrane targeting of stromal interaction molecule 1 after Ca2+ store depletion. *Proc Natl Acad Sci U S A* **104**, 9301–9306 (2007).
76. Maléth, J., Choi, S., Muallem, S. & Ahuja, M. Translocation between PI(4,5)P2-poor and PI(4,5)P2-rich microdomains during store depletion determines STIM1 conformation and Orai1 gating. *Nat Commun* **5**, 5843 (2014).
77. Ma, G. *et al.* Optogenetic engineering to probe the molecular choreography of STIM1-mediated cell signaling. *Nat Commun* **11**, 1039 (2020).
78. Fujii, Y. *et al.* Surf4 modulates STIM1-dependent calcium entry. *Biochem Biophys Res Commun* **422**, 615–620 (2012).
79. Quintana, A. *et al.* TMEM110 regulates the maintenance and remodeling of mammalian ER-plasma membrane junctions competent for STIM-ORAI signaling. *Proc Natl Acad Sci U S A* **112**, E7083-92 (2015).
80. Srikanth, S. *et al.* A novel EF-hand protein, CRACR2A, is a cytosolic Ca2+ sensor that stabilizes CRAC channels in T cells. *Nat Cell Biol* **12**, 436–446 (2010).
81. Walsh, C. M., Doherty, M. K., Tepikin, A. v & Burgoyne, R. D. Evidence for an interaction between Golli and STIM1 in store-operated calcium entry. *Biochem J* **430**, 453–460 (2010).
82. Zeiger, W. *et al.* Stanniocalcin 2 is a negative modulator of store-operated calcium entry. *Mol Cell Biol* **31**, 3710–3722 (2011).
83. Carreras-Sureda, A. *et al.* ORMDL3 modulates store-operated calcium entry and lymphocyte activation. *Hum Mol Genet* **22**, 519–530 (2013).
84. Lopez, E. *et al.* STIM1 phosphorylation at Y316 modulates its interaction with SARAF and the activation of SOCE and ICRAC. *J Cell Sci* **132**, (2019).
85. Albarran, L. *et al.* Dynamic interaction of SARAF with STIM1 and Orai1 to modulate store-operated calcium entry. *Sci Rep* **6**, (2016).
86. Albarran, L. *et al.* EFHB is a novel cytosolic Ca 2+ sensor that modulates STIM1-SARAF interaction. *Cellular Physiology and Biochemistry* **51**, 1164–1178 (2018).
87. Yang, S., Zhang, J. J. & Huang, X. Y. Orai1 and STIM1 are critical for breast tumor cell migration and metastasis. *Cancer Cell* **15**, 124–134 (2009).
88. Lee, S. K., Kweon, Y. C., Lee, A. R., Lee, Y. Y. & Park, C. Y. Metastasis enhancer PGRMC1 boosts store-operated Ca2+ entry by uncoiling Ca2+ sensor STIM1 for focal adhesion turnover and actomyosin formation. *Cell Rep* **38**, 110281 (2022).

89. Kimberlin, C. R. *et al.* SARAF Luminal Domain Structure Reveals a Novel Domain-Swapped β-Sandwich Fold Important for SOCE Modulation. *J Mol Biol* **431**, 2869–2883 (2019).
90. Tang, Z. *et al.* GEPIA: a web server for cancer and normal gene expression profiling and interactive analyses. *Nucleic Acids Res* **45**, W98–W102 (2017).
91. Rivas, J. *et al.* KCTD5, a novel TRPM4-regulatory protein required for cell migration as a new predictor for breast cancer prognosis. *FASEB Journal* (2020) doi:10.1096/fj.201901195RRR.
92. Mattheyses, A. L., Simon, S. M. & Rappoport, J. Z. Imaging with total internal reflection fluorescence microscopy for the cell biologist. *J Cell Sci* **123**, 3621–3628 (2010).
93. Cáceres, M. *et al.* TRPM4 Is a Novel Component of the Adhesome Required for Focal Adhesion Disassembly, Migration and Contractility. *PLoS One* **10**, e0130540 (2015).
94. Prakriya, M. *et al.* Orai1 is an essential pore subunit of the CRAC channel. *Nature* **443**, 230–233 (2006).
95. Herbert, A. D., Carr, A. M., Hoffmann, E. & Lichten, M. FindFoci: A Focus Detection Algorithm with Automated Parameter Training That Closely Matches Human Assignments, Reduces Human Inconsistencies and Increases Speed of Analysis. *PLoS One* **9**, e114749 (2014).
96. Kar, P., Nelson, C. & Parekh, A. B. Selective Activation of the Transcription Factor NFAT1 by Calcium Microdomains near Ca2+ Release-activated Ca2+ (CRAC) Channels. *Journal of Biological Chemistry* **286**, 14795–14803 (2011).
97. Goetz, J. G. *et al.* Concerted regulation of focal adhesion dynamics by galectin-3 and tyrosine-phosphorylated caveolin-1. *Journal of Cell Biology* **180**, 1261–1275 (2008).
98. Canales, J. *et al.* K+ Channel Tetramerization Domain 5 (KCTD5) Protein Regulates Cell Migration, Focal Adhesion Dynamics and Spreading through Modulation of Ca2+ Signaling and Rac1 Activity. *Cells* **9**, 2273 (2020).
99. Blanco, C. *et al.* EB1- and EB2-dependent anterograde trafficking of TRPM4 regulates focal adhesion turnover and cell invasion. *FASEB J* **33**, 9434–9452 (2019).
100. Ghosh, A. *et al.* MIND model for triple-negative breast cancer in syngeneic mice for quick and sequential progression analysis of lung metastasis. *PLoS One* **13**, e0198143 (2018).
101. Sápi, J. *et al.* Tumor Volume Estimation and Quasi-Continuous Administration for Most Effective Bevacizumab Therapy. *PLoS One* **10**, e0142190 (2015).
102. Salgado, R. *et al.* The evaluation of tumor-infiltrating lymphocytes (TILs) in breast cancer: recommendations by an International TILs Working Group 2014. *Annals of Oncology* **26**, 259–271 (2015).
103. Lord, S. J., Velle, K. B., Mullins, R. D. & Fritz-Laylin, L. K. SuperPlots: Communicating reproducibility and variability in cell biology. *Journal of Cell Biology* **219**, (2020).
104. Park, C. Y. *et al.* STIM1 Clusters and Activates CRAC Channels via Direct Binding of a Cytosolic Domain to Orai1. *Cell* **136**, 876–890 (2009).

105. Kerppola, T. K. Design and implementation of bimolecular fluorescence complementation (BiFC) assays for the visualization of protein interactions in living cells. *Nat Protoc* **1**, 1278–1286 (2006).
106. Hertel, F., Mo, G. C. H., Duwé, S., Dedecker, P. & Zhang, J. RefSOFI for Mapping Nanoscale Organization of Protein-Protein Interactions in Living Cells. *Cell Rep* **14**, 390–400 (2016).
107. Zhou, M.-H. *et al.* Stromal Interaction Molecule 1 (STIM1) and Orai1 Mediate Histamine-evoked Calcium Entry and Nuclear Factor of Activated T-cells (NFAT) Signaling in Human Umbilical Vein Endothelial Cells. *Journal of Biological Chemistry* **289**, 29446–29456 (2014).
108. Müller, M. R. & Rao, A. NFAT, immunity and cancer: a transcription factor comes of age. *Nature Reviews Immunology 2010 10:9* **10**, 645–656 (2010).
109. Tran Quang, C. *et al.* The calcineurin/NFAT pathway is activated in diagnostic breast cancer cases and is essential to survival and metastasis of mammary cancer cells. *Cell Death & Disease 2015 6:2* **6**, e1658–e1658 (2015).
110. Chen, Y. F., Lin, P. C., Yeh, Y. M., Chen, L. H. & Shen, M. R. Store-Operated Ca2+ entry in tumor progression: From molecular mechanisms to clinical implications. *Cancers* vol. 11 899 Preprint at https://doi.org/10.3390/cancers11070899 (2019).
111. Carragher, N. O. & Frame, M. C. Focal adhesion and actin dynamics: a place where kinases and proteases meet to promote invasion. *Trends Cell Biol* **14**, 241–249 (2004).
112. Tian, C., Du, L., Zhou, Y. & Li, M. Store-operated CRAC channel inhibitors: opportunities and challenges. *Future Med Chem* **8**, 817–832 (2016).
113. Schulte, U., Müller, C. S. & Fakler, B. Ion channels and their molecular environments--glimpses and insights from functional proteomics. *Semin Cell Dev Biol* **22**, 132–144 (2011).
114. Schulte, U. Protein-protein interactions and subunit composition of ion channels. *CNS Neurol Disord Drug Targets* **7**, 172–186 (2008).
115. Stoilova-McPhie, S., Ali, S. & Laezza, F. Protein-Protein Interactions as New Targets for Ion Channel Drug Discovery. *Austin J Pharmacol Ther* **1**, (2013).
116. Lu, H. *et al.* Recent advances in the development of protein–protein interactions modulators: mechanisms and clinical trials. *Signal Transduction and Targeted Therapy 2020 5:1* **5**, 1–23 (2020).
117. Baraniak, J. H. *et al.* Orai channel C-terminal peptides are key modulators of STIM-Orai coupling and calcium signal generation. *Cell Rep* **35**, 109322 (2021).
118. Patel, S. G. *et al.* Cell-penetrating peptide sequence and modification dependent uptake and subcellular distribution of green florescent protein in different cell lines. *Scientific Reports 2019 9:1* **9**, 1–9 (2019).
119. Wadia, J. S., Stan, R. v & Dowdy, S. F. Transducible TAT-HA fusogenic peptide enhances escape of TAT-fusion proteins after lipid raft macropinocytosis. *Nat Med* **10**, 310–315 (2004).
120. Teesalu, T., Sugahara, K. N. & Ruoslahti, E. Tumor-penetrating peptides. *Front Oncol* **3**, 216 (2013).
121. Dong, X., Liu, L., Zhu, D., Zhang, H. & Leng, X. Transactivator of transcription (TAT) peptide- chitosan functionalized multiwalled carbon nanotubes as a

potential drug delivery vehicle for cancer therapy. *Int J Nanomedicine* **10**, 3829–3841 (2015).
122. Hsieh, T. H. *et al.* A novel cell-penetrating peptide suppresses breast tumorigenesis by inhibiting β-catenin/LEF-1 signaling. *Scientific Reports 2016 6:1* **6**, 1–12 (2016).
123. Gheybi, F. *et al.* pH-Sensitive PEGylated Liposomal Silybin: Synthesis, In Vitro and In Vivo Anti-Tumor Evaluation. *J Pharm Sci* **110**, 3919–3928 (2021).
124. Sanchez-Collado, J. *et al.* Orai2 modulates store-operated ca2+ entry and cell cycle progression in breast cancer cells. *Cancers (Basel)* **14**, (2022).
125. Zhang, L.-Y. *et al.* TRPC1 inhibits the proliferation and migration of estrogen receptor-positive Breast cancer and gives a better prognosis by inhibiting the PI3K/AKT pathway. *Breast Cancer Res Treat* **182**, 21–33 (2020).
126. el Hiani, Y., Lehen'kyi, V., Ouadid-Ahidouch, H. & Ahidouch, A. Activation of the calcium-sensing receptor by high calcium induced breast cancer cell proliferation and TRPC1 cation channel over-expression potentially through EGFR pathways. *Arch Biochem Biophys* **486**, 58–63 (2009).
127. Jardin, I. *et al.* Melatonin downregulates TRPC6, impairing store-operated calcium entry in triple-negative breast cancer cells. *Journal of Biological Chemistry* **296**, 100254 (2021).
128. Zhang, H. *et al.* Comprehensive Analysis of TRP Channel–Related Genes in Patients With Triple-Negative Breast Cancer for Guiding Prognostic Prediction. *Front Oncol* **12**, (2022).
129. Jardin, I. *et al.* Trpc6 channels are required for proliferation, migration and invasion of breast cancer cell lines by modulation of orai1 and orai3 surface exposure. *Cancers (Basel)* (2018) doi:10.3390/cancers10090331.
130. Yang, Y. *et al.* Expression of STIM1 is associated with tumor aggressiveness and poor prognosis in breast cancer. *Pathol Res Pract* **213**, (2017).
131. Cheng, H., Wang, S. & Feng, R. STIM1 plays an important role in TGF-β-induced suppression of breast cancer cell proliferation. *Oncotarget* **7**, 16866–16878 (2016).
132. Zhang, S. *et al.* STIM1 and STIM2 differently regulate endogenous Ca2+ entry and promote TGF-β-induced EMT in breast cancer cells. *Biochem Biophys Res Commun* **488**, 74–80 (2017).
133. Kimberlin, C. R. *et al.* SARAF Luminal Domain Structure Reveals a Novel Domain-Swapped β-Sandwich Fold Important for SOCE Modulation. *J Mol Biol* **431**, 2869–2883 (2019).
134. Yen, M., Lokteva, L. A. & Lewis, R. S. Functional Analysis of Orai1 Concatemers Supports a Hexameric Stoichiometry for the CRAC Channel. *Biophys J* (2016) doi:10.1016/j.bpj.2016.09.020.
135. Yen, M. & Lewis, R. S. Numbers count: How STIM and Orai stoichiometry affect store-operated calcium entry. *Cell Calcium* vol. 79 Preprint at https://doi.org/10.1016/j.ceca.2019.02.002 (2019).
136. Albarran, L., Lopez, J. J., Woodard, G. E., Salido, G. M. & Rosado, J. A. Store-operated Ca2+ entry- Associated regulatory factor (SARAF) plays an important role in the regulation of arachidonate-regulated Ca2+ (ARC) channels. *Journal of Biological Chemistry* **291**, 6982–6988 (2016).

137. Tang, S. *et al.* Mitochondrial Ca2+ uniporter is critical for store-operated Ca2+ entry-dependent breast cancer cell migration. *Biochem Biophys Res Commun* **458**, 186–193 (2015).
138. Jardin, I. *et al.* SARAF and EFHB Modulate Store-Operated Ca 2+ Entry and Are Required for Cell Proliferation, Migration and Viability in Breast Cancer Cells. (2021) doi:10.3390/cancers.
139. Dupont, G., Combettes, L., Bird, G. S. & Putney, J. W. Calcium Oscillations. *Cold Spring Harb Perspect Biol* **3**, a004226–a004226 (2011).
140. Wedel, B., Boyles, R. R., Putney, J. W. & Bird, G. S. Role of the store-operated calcium entry proteins Stim1 and Orai1 in muscarinic cholinergic receptor-stimulated calcium oscillations in human embryonic kidney cells. *J Physiol* **579**, 679–689 (2007).
141. Bird, G. S. *et al.* STIM1 is a calcium sensor specialized for digital signaling. *Curr Biol* **19**, 1724–1729 (2009).
142. Emrich, S. M. *et al.* Omnitemporal choreographies of all five STIM/Orai and IP3Rs underlie the complexity of mammalian Ca2+ signaling. *Cell Rep* **34**, 108760 (2021).
143. Subedi, K. P., Ong, H. L., Son, G.-Y., Liu, X. & Ambudkar, I. S. STIM2 Induces Activated Conformation of STIM1 to Control Orai1 Function in ER-PM Junctions. *Cell Rep* **23**, 522–534 (2018).
144. Chamlali, M., Rodat-Despoix, L. & Ouadid-Ahidouch, H. Store-independent calcium entry and related signaling pathways in breast cancer. *Genes (Basel)* **12**, (2021).
145. Cantonero, C. *et al.* Store-independent Orai1-mediated Ca 2+ entry and cancer. *Cell Calcium* **80**, 1–7 (2019).
146. Mignen, O., Thompson, J. L. & Shuttleworth, T. J. The molecular architecture of the arachidonate-regulated Ca2+-selective ARC channel is a pentameric assembly of Orai1 and Orai3 subunits. *J Physiol* **587**, 4181 (2009).
147. Mignen, O., Thompson, J. L. & Shuttleworth, T. J. Both Orai1 and Orai3 are essential components of the arachidonate-regulated Ca2+-selective (ARC) channels. *J Physiol* **586**, 185 (2008).
148. Chamlali, M. *et al.* Orai3 calcium channel regulates breast cancer cell migration through calcium-dependent and-independent mechanisms. *Cells* **10**, 3487 (2021).
149. Feng, M. *et al.* Store-independent activation of orai1 by SPCA2 in mammary tumors. *Cell* **143**, 84–98 (2010).
150. Peretti, M. *et al.* Original association of ion transporters mediates the ECM-induced breast cancer cell survival: Kv10.1-Orai1-SPCA2 partnership. *Sci Rep* **9**, (2019).
151. Girault, A. *et al.* The N and C-termini of SPCA2 regulate differently Kv10.1 function: role in the collagen 1-induced breast cancer cell survival. *Am J Cancer Res* **11**, 251 (2021).
152. Gueguinou, M. *et al.* The SigmaR1 chaperone drives breast and colorectal cancer cell migration by tuning SK3-dependent Ca2+ homeostasis. *Oncogene 2017 36:25* **36**, 3640–3647 (2017).

153. Clarysse, L. *et al.* cAMP-PKA inhibition of SK3 channel reduced both Ca2+ entry and cancer cell migration by regulation of SK3-Orai1 complex. *Pflugers Arch* **466**, 1921–1932 (2014).
154. Potier, M. *et al.* Identification of SK3 channel as a new mediator of breast cancer cell migration. *Mol Cancer Ther* **5**, 2946–2953 (2006).
155. Tiffner, A. *et al.* Orai1 boosts sk3 channel activation. *Cancers (Basel)* **13**, 6357 (2021).
156. Cantonero, C., Camello, P. J., Salido, G. M., Rosado, J. A. & Redondo, P. C. TMEM97 facilitates the activation of SOCE by downregulating the association of cholesterol to Orai1 in MDA-MB-231 cells. *Biochim Biophys Acta Mol Cell Biol Lipids* **1866**, (2021).
157. Sanchez-Collado, J. *et al.* Adenylyl cyclase type 8 overexpression impairs phosphorylation-dependent orai1 inactivation and promotes migration in MDA-MB-231 breast cancer cells. *Cancers (Basel)* **11**, (2019).
158. Dyrda, A., Koenig, S. & Frieden, M. STIM1 long and STIM1 gate differently TRPC1 during store-operated calcium entry. *Cell Calcium* **86**, 102134 (2020).
159. Stewart, T. A. *et al.* Differential engagement of ORAI1 and TRPC1 in the induction of vimentin expression by different stimuli. *Laboratory Investigation* **100**, 224–233 (2020).
160. Lin, Y. P., Bakowski, D., Mirams, G. R. & Parekh, A. B. Selective recruitment of different Ca2+-dependent transcription factors by STIM1-Orai1 channel clusters. *Nat Commun* **10**, (2019).
161. Bayón, Y. *et al.* KCTD5, a putative substrate adaptor for cullin3 ubiquitin ligases. *FEBS J* **275**, 3900–3910 (2008).
162. Cheng, J. *et al.* Functional analysis of Cullin 3 E3 ligases in tumorigenesis. *Biochimica et Biophysica Acta (BBA) - Reviews on Cancer* **1869**, 11–28 (2018).
163. Gong, L., Cui, D., Xiong, X. & Zhao, Y. Targeting Cullin-RING Ubiquitin Ligases and the Applications in PROTACs. in 317–347 (2020). doi:10.1007/978-981-15-1025-0_19.
164. Liu, X. *et al.* Orai1 is critical for Notch-driven aggressiveness under hypoxic conditions in triple-negative breast cancers. *Biochim Biophys Acta Mol Basis Dis* **1864**, 975–986 (2018).
165. Chakraborty, S. *et al.* Phemindole, a synthetic di-indole derivative maneuvers the Store Operated Calcium Entry (SOCE) to induce potent anti-carcinogenic activity in human triple negative breast cancer cells. *Front Pharmacol* **7**, (2016).
166. Luan, H. *et al.* EHD2 overexpression promotes tumorigenesis and metastasis in triple-negative breast cancer by regulating store-operated calcium entry Introduction. doi:10.1101/2022.06.21.497035.
167. Jeon, I. S. *et al.* Modulation of store-operated calcium entry and nascent adhesion by p21-activated kinase 1. *Exp Mol Med* **50**, (2018).
168. Saldivar-Cerón, H. I. *et al.* p21-Activated Kinase 1 Promotes Breast Tumorigenesis via Phosphorylation and Activation of the Calcium/Calmodulin-Dependent Protein Kinase II. *Front Cell Dev Biol* **9**, (2022).
169. Sun, J. *et al.* STIM1- and Orai1-mediated Ca2+ oscillation orchestrates invadopodium formation and melanoma invasion. *Journal of Cell Biology* **207**, 535–548 (2014).

170. Siddiqui, T. A., Lively, S., Vincent, C. & Schlichter, L. C. Regulation of podosome formation, microglial migration and invasion by Ca2+-signaling molecules expressed in podosomes. *J Neuroinflammation* **9**, (2012).
171. Rizaner, N. *et al.* Intracellular calcium oscillations in strongly metastatic human breast and prostate cancer cells: control by voltage-gated sodium channel activity. *European Biophysics Journal* **45**, 735–748 (2016).
172. Chen, Y. T. *et al.* The ER Ca2+ sensor STIM1 regulates actomyosin contractility of migratory cells. *J Cell Sci* **126**, 1260–1267 (2013).
173. Loi, S. *et al.* Tumor infiltrating lymphocyte stratification of prognostic staging of early-stage triple negative breast cancer. *NPJ Breast Cancer* **8**, 3 (2022).
174. Schosserer, M., Grillari, J. & Breitenbach, M. The Dual Role of Cellular Senescence in Developing Tumors and Their Response to Cancer Therapy. *Front Oncol* **7**, 278 (2017).
175. Xu, Y. *et al.* STIM1 accelerates cell senescence in a remodeled microenvironment but enhances the epithelial-to-mesenchymal transition in prostate cancer. *Sci Rep* **5**, 1–17 (2015).
176. Gatti, G. *et al.* High IRF8 expression correlates with CD8 T cell infiltration and is a predictive biomarker of therapy response in ER-negative breast cancer. *Breast Cancer Res* **23**, (2021).